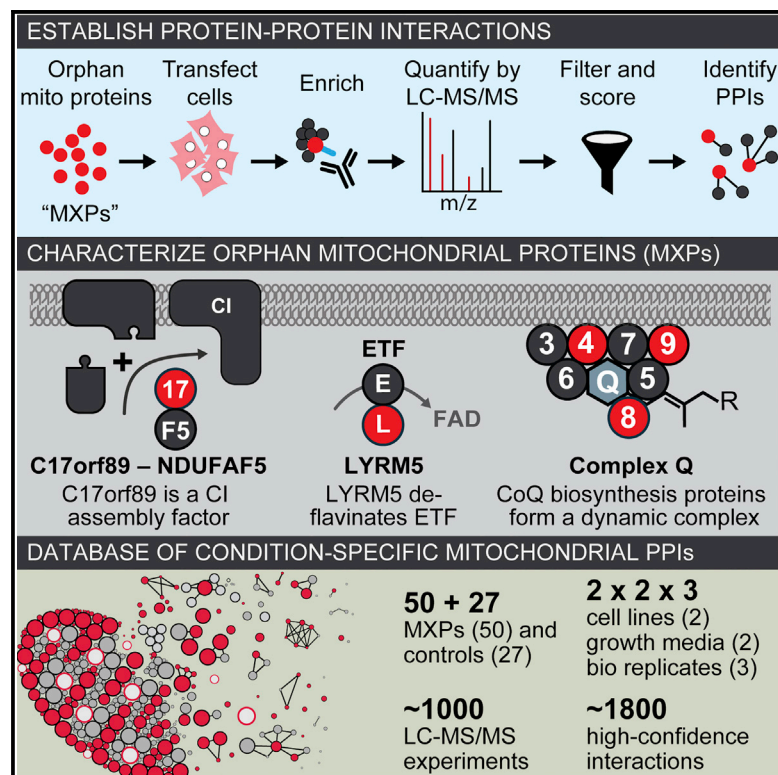


Mitochondrial Protein Interaction Mapping Identifies Regulators of Respiratory Chain Function

Graphical Abstract



Authors

Brendan J. Floyd, Emily M. Wilkerson, Mike T. Veling, ..., Jung-Ja P. Kim, Joshua J. Coon, David J. Pagliarini

Correspondence

dpagliarini@morgridge.org

In Brief

Mitochondria are essential organelles, yet hundreds of their proteins lack robust functional characterization. Floyd et al. (2016) define interaction partners for 50 such proteins, providing hypotheses about their roles in mitochondria. In particular, their work lends mechanistic insight into respiratory chain activities related to complex I, the electron transferring flavoprotein, and coenzyme Q.

Highlights

- PPI mapping of 50 MXPs reveals mitochondrial protein functions
- C17orf89 is a CI assembly factor depleted in a case of CI deficiency
- LYRM5 interacts with and deflavinate the electron transferring flavoprotein
- Proteins involved in coenzyme Q biosynthesis form a dynamic “complex Q”

Mitochondrial Protein Interaction Mapping Identifies Regulators of Respiratory Chain Function

Brendan J. Floyd,^{1,2,10} Emily M. Wilkerson,^{3,10} Mike T. Veling,^{1,2,10} Catie E. Minogue,^{3,10} Chuanwu Xia,⁴ Emily T. Beebe,² Russell L. Wrobel,² Holly Cho,^{1,2} Laura S. Kremer,^{5,6} Charlotte L. Alston,⁷ Katarzyna A. Gromek,² Brendan K. Dolan,² Arne Ulbrich,³ Jonathan A. Stefely,^{1,2} Sarah L. Bohl,^{1,2} Kelly M. Werner,² Adam Jochem,¹ Michael S. Westphall,⁹ Jarred W. Rensvold,¹ Robert W. Taylor,⁷ Holger Prokisch,^{5,6} Jung-Ja P. Kim,⁴ Joshua J. Coon,^{3,8,9} and David J. Pagliarini^{1,2,*}

¹Morgridge Institute for Research, Madison, WI 53715, USA

²Department of Biochemistry

³Department of Chemistry

University of Wisconsin–Madison, Madison, WI 53706, USA

⁴Department of Biochemistry, Medical College of Wisconsin, Milwaukee, WI 53226, USA

⁵Institute of Human Genetics, Technische Universität München, 81675 München, Germany

⁶Institute of Human Genetics, Helmholtz Zentrum München, 85764 Neuherberg, Germany

⁷Wellcome Trust Centre for Mitochondrial Research, Institute of Neuroscience, The Medical School, Newcastle University, Newcastle upon Tyne NE2 4HH, UK

⁸Department of Biomolecular Chemistry

⁹Genome Center of Wisconsin

University of Wisconsin–Madison, Madison, WI 53706, USA

¹⁰Co-first author

*Correspondence: dpagliarini@morgridge.org

<http://dx.doi.org/10.1016/j.molcel.2016.06.033>

SUMMARY

Mitochondria are essential for numerous cellular processes, yet hundreds of their proteins lack robust functional annotation. To reveal functions for these proteins (termed MXPs), we assessed condition-specific protein-protein interactions for 50 select MXPs using affinity enrichment mass spectrometry. Our data connect MXPs to diverse mitochondrial processes, including multiple aspects of respiratory chain function. Building upon these observations, we validated C17orf89 as a complex I (CI) assembly factor. Disruption of C17orf89 markedly reduced CI activity, and its depletion is found in an unresolved case of CI deficiency. We likewise discovered that LYRM5 interacts with and deflavinates the electron-transferring flavoprotein that shuttles electrons to coenzyme Q (CoQ). Finally, we identified a dynamic human CoQ biosynthetic complex involving multiple MXPs whose topology we map using purified components. Collectively, our data lend mechanistic insight into respiratory chain-related activities and prioritize hundreds of additional interactions for further exploration of mitochondrial protein function.

INTRODUCTION

Mitochondria are centers of metabolism for nearly all eukaryotic cells. Once considered to be mere sites of ATP generation, it is now appreciated that mitochondria participate in a wide range of essential functions related to cellular metabolism, signaling, and programmed cell death (Pagliarini and Rutter, 2013). Consistently, large-scale proteomics- and computation-based efforts during the past decade have revealed that the mitochondrial proteome is much more extensive than once thought, and dysfunction of these organelles is now associated with hundreds of inborn errors of metabolism and common diseases (Koopman et al., 2012; Nunnari and Suomalainen, 2012).

Despite our advanced cataloging of the mammalian mitochondrial proteome, functional characterization of these proteins is far from complete (Calvo et al., 2016; Pagliarini et al., 2008). This gap in knowledge has limited our understanding of basic mitochondrial biology and has obscured the nature and cause of many mitochondrial diseases. For instance, many patients with biochemically established mitochondrial diseases lack mutations in known mitochondrial disease genes, implying the existence of unidentified proteins whose proper functions are necessary for the affected processes (Calvo et al., 2010; Haack et al., 2011). Alternatively, other diseases arise from mutations in mitochondrial proteins with no known functions, making it difficult to interrogate the molecular mechanisms of the diseases.

Protein-protein interactions (PPIs) can provide powerful insight into protein function. Recent advancements in affinity enrichment mass spectrometry (AE-MS) (Hein et al., 2015;

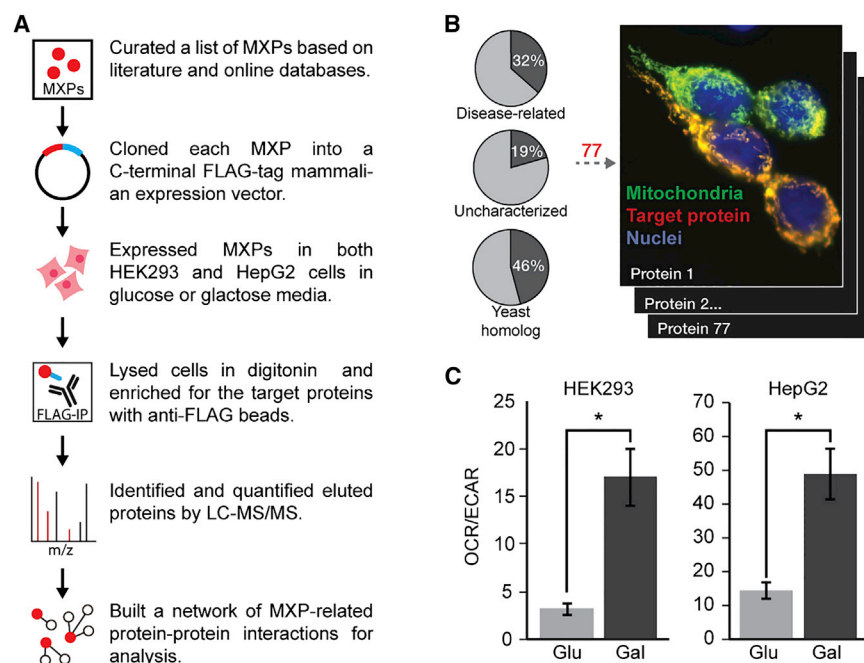


Figure 1. AE-MS Methodology

(A) Schematic workflow of the AE-MS method. (B) Localization of all FLAG-tagged constructs was established based on MLS-GFP and anti-FLAG fluorescence microscopy (see Figure S1). Venn diagrams report the percentage of the MitoCarta+ list (Table S1) associated with each category. (C) Galactose induces mitochondrial respiration. Ratio of rates of oxygen consumption (OCR) and extracellular acidification (ECAR) in HEK293 (left) and HepG2 (right) cells grown in 10 mM glucose (Glu) or galactose (Gal) for 24 hr prior to assay. OCR/ECAR is proportional to mitochondrial versus glycolytic flux (asterisk indicates t test $p < 0.05$). Error bars indicate \pm SEM.

RESULTS

At Least 20% of the Mitochondrial Proteome Lacks Functional Annotation

Previous analyses have suggested that much of the mitochondrial proteome is uncharacterized (Pagliarini et al., 2008;

Pagliarini and Rutter, 2013). To capture an up-to-date assessment of mitochondrial proteins and their functions, we combined the recently updated MitoCarta 2.0 list (Calvo et al., 2016) with additional literature sources to generate a MitoCarta+ list of 1,166 human proteins with validated mitochondrial localization (see Table S1 available online). Next, we annotated these proteins based on the integration of online databases and analysis of the current literature (see Experimental Procedures). Our data indicate that at least 228 mitochondrial proteins have no known, or poorly established, biochemical function, and that an additional 26 proteins with dual localization to the mitochondrion and another cellular compartment do not have clear roles within the mitochondrion. These MXPs constitute ~20% of the mammalian mitochondrial proteome and include many proteins associated with human disease (Table S1; Supplemental Experimental Procedures).

Overall Experimental Strategy

To begin characterizing the functions of MXPs, we elected to establish MXP-specific interactions via AE-MS—an approach proven to be capable of efficiently connecting uncharacterized proteins to known pathways (Figure 1A). We prioritized an initial set of 50 MXPs (Table S1) based on disease relevance, evolutionary conservation, and confirmed localization to mitochondria when possessing a C-terminal FLAG-tag (Figures 1B and S1). We supplemented these bait proteins with 27 mitochondrial proteins of known function (Table S1) and a variant of green fluorescent protein harboring an N-terminal mitochondrial localization sequence (MLS-GFP-FLAG). We performed our interaction analyses in two cell lines (HEK293 and HepG2) grown in both glucose- and galactose-based media conditions. Galactose is known to increase oxygen consumption and dependence on mitochondrial respiratory chain function, which we observed in both lines (Figure 1C). We collected three replicates (i.e., distinct

Hosp et al., 2015; Huttlin et al., 2015; Keilhauer et al., 2015) have improved the ability to accurately detect PPIs, enabling researchers to overcome the systematic bias against poorly characterized proteins inherent in many large-scale “interactome” analyses (Sahni et al., 2015). With AE-MS, a protein of interest (i.e., the bait) is enriched from a sample; it and any co-enriching proteins are then analyzed by mass spectrometry (MS). In this process, the majority of captured proteins are typically not meaningful interactors of the bait. To sort the so-called wheat from the chaff, the AE-MS approach combines the analyses of multiple baits with a robust quantitative MS platform and a scoring algorithm to differentiate between informative interactions and nonspecific background co-enrichment.

In this study, we began by curating a list of proteins from the mitochondrial proteome that lack significant functional annotation, which we call mitochondrial uncharacterized (x) proteins (MXPs). Using stringent criteria, we conservatively estimate there to be 228 MXPs in humans, including more than 25 that have been associated with human diseases. We then designed a robust AE-MS strategy to define an extensive cell type- and condition-specific interactome of 50 select MXPs, enabling us to propose functions and disease associations for these uncharacterized proteins.

Informed by our large-scale AE-MS analyses, we conducted extensive in vitro biochemistry and cell biology experiments that validated roles for MXPs in various aspects of the mitochondrial respiratory chain. We establish C17orf89 as a complex I (CI) assembly factor, whose silencing markedly impairs CI activity, and whose depletion is found in an unresolved case of isolated CI deficiency. We also establish LYRM5 as a “deflavinase” that directly regulates the electron transferring flavoprotein (ETF) and identify a dynamic human coenzyme Q biosynthetic complex that includes multiple MXPs. We propose functions for a variety of other MXPs and make our data freely available to the community to accelerate further annotation of mitochondrial proteins.

cell transfections) of each condition for a total of 12 analyses per bait protein.

Following anti-FLAG immunoaffinity enrichment, protein eluate was analyzed using nanoflow liquid chromatography coupled to high-resolution MS (quadrupole linear ion trap-Orbitrap hybrid, nLC-MS/MS). Analysis of these 78 unique baits required 936 nLC-MS/MS experiments that generated 20 million MS/MS spectra, identified 5 million unique peptides, and resulted in the observation of 10,000 unique proteins. On average, each nLC-MS/MS experiment detected ~1,000 unique proteins; however, each bait likely has far fewer bona fide interactions. To help distinguish genuine interactions from background, we utilized CompPASS, a known and validated algorithmic approach for highlighting high-confidence interactions and removing non-specific binders (Sowa et al., 2009), modified to incorporate label-free quantitation data.

AE-MS Analyses Identify Hundreds of Mitochondrial Protein Interactions

To assess the performance of our approach and to determine an appropriate cutoff score, we focused on our positive-control bait proteins that have known binding partners. We curated a list of literature-established PPIs involving our positive-control baits and compared their CompPASS scores to those for all mitochondrial preys (Table S2). We selected a stringent cutoff score that achieved 93% sensitivity for known PPIs while simultaneously eliminating 95% of all observed, likely background, interactions (Figure 2A).

Applying this threshold to the rest of our data, and filtering for proteins in our MitoCarta+ list, we identified 1,829 interactions from a total observed set of 109,817 (Figure 2B; Table S3). Consistent with previous efforts (Jäger et al., 2012), we found that using more than one cell type is an effective means for identifying and prioritizing interactions, as only 32% of interactions are shared between the cell lines when limited to our stringent cutoff score (Figure 2C). Changing the carbon source (i.e., glucose versus galactose) had a more modest effect, with 61% of interactions shared between conditions at our threshold cutoff (Figures 2D and S2); however, the abundances of hundreds of these shared interactions are modulated by these changing conditions (Figure 2E), suggesting that mitochondrial metabolism may be linked to the regulation of PPIs. Thus, our experimental design expanded our search space, enabled the identification of meaningful interactions by excluding nonspecific background, and detected interactions affected by nutrient state.

C17orf89 Is a CI Assembly Factor

We designed our study with an awareness that many known mitochondrial pathways and processes are “missing” enzymes or functional components that could be completed by our MXP. For example, 45%–60% of biochemically validated cases of CI (Calvo et al., 2010; Haack et al., 2011), CII (Jain-Ghai et al., 2013), and CIII deficiency (Fernández-Vizarra and Zeviani, 2015) lack molecular diagnoses. As such, we prioritized MXPs that interacted with respiratory chain components for functional investigations.

A particularly noteworthy MXP in this category was C17orf89, a 7 kDa protein that interacted with the known CI assembly factor

(CIAF) NDUFAF5 (Figure 3A). Out of 1,415 observed preys for C17orf89, 31 mitochondrial proteins were above our cutoff score, and only four interactions were observed in both cell lines. Of these, the highest-scoring interaction was between C17orf89 and NDUFAF5. Reciprocally, only three mitochondrial preys interacted with NDUFAF5 in both cell lines, one of which was C17orf89. We validated this C17orf89-NDUFAF5 interaction by showing that immunoprecipitation of FLAG-tagged C17orf89 from HEK293 cells captured endogenous NDUFAF5 (Figure 3B).

To test the hypothesis that C17orf89 is necessary for CI activity, we used RNAi to knock down (KD) *C17orf89* expression in HEK293 cells via lentiviral shRNA constructs. Indeed, we found that silencing of *C17orf89* had a dramatic effect on CI activity (Figure 3C) and subunit levels (Figure S3A), with no consistent change in the abundance of subunits of other respiratory chain complexes. We also observed a slight decrease in the abundance of a subunit of CIV (Figure S3A) and of CIV activity (Figure S3B), consistent with a recent study suggesting that loss of NDUFAF5 also perturbs CIV (Saada et al., 2012). We further observed a dramatic reduction in the oxygen consumption rates of live *C17orf89* KD cells, both basally and upon stimulation with the uncoupler FCCP (Figure 3D), without change to the extracellular acidification rate (ECAR, a measure of glycolytic activity) (Figure S3C). Notably, transfection of *C17orf89*-FLAG, but not GFP-FLAG, into KD cell lines was able to rescue much of the lost CI activity (Figure 3E).

To further assess the functional relationship between C17orf89 and NDUFAF5, we established siRNA-mediated HEK293 KD of *C17orf89*, *NDUFAF4*, *NDUFAF5*, *NDUFAF6*, and the CI subunit *NDUFS3* (Figures S4A–S4E) and analyzed each using MS. Silencing of the target genes resulted in an overall decrease in CI subunits; however, the pattern of subunit changes for the *C17orf89* kd cells was most similar to that of *NDUFAF5* (Figure S4F), further strengthening the C17orf89-NDUFAF5 functional relationship. Strikingly, silencing of *C17orf89*, but not other CIAFs or *NDUFS3*, resulted in a drastic loss of NDUFAF5 protein (Figure 4A), suggesting that the role of C17orf89 in CI assembly likely involves the direct stabilization of NDUFAF5.

Our implication of C17orf89 as a CI assembly factor motivated us to investigate the possibility that its disruption might contribute to unresolved patient cases of isolated CI deficiency. We sequenced *C17orf89* in 125 such cases but did not identify likely pathogenic variants. However, RNaseq analysis on 96 cell lines from mitochondrial disease patients that had previously been analyzed by whole-exome sequencing revealed one case that exhibited an 80% reduction of *C17orf89* reads (Figure 4B). This patient, now 26 years of age, was born to unrelated parents and presented in childhood with acute encephalopathy, seizures, mild spasticity, and neuroradiological features consistent with a diagnosis of Leigh syndrome (bilateral high signal intensities in the basal ganglia and brainstem); a diagnostic muscle biopsy at the age of 14 revealed evidence of an isolated CI defect (<40% control activity; Figure 4C). Respiratory chain activities were normal in the sequenced cultured skin fibroblasts (Figure S4G), as is the case for ~50% of patients exhibiting a respiratory chain defect detected in skeletal muscle, liver, or heart (Kirby et al., 2007), thereby precluding our ability to rescue the defect by reintroduction of wild-type *C17orf89*.

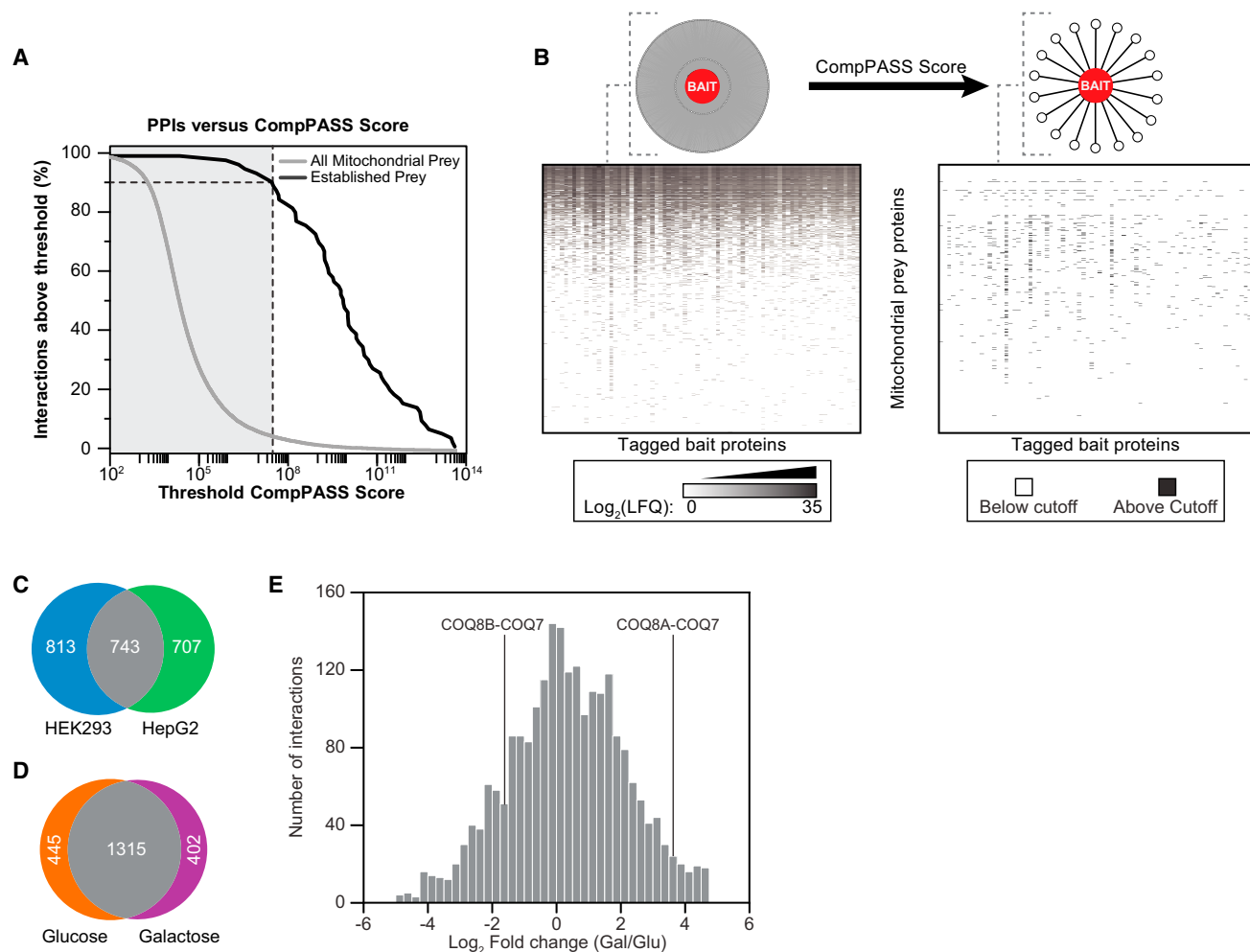


Figure 2. Overall Analyses of Our AE-MS Approach

(A) CompPASS scoring accuracy. CompPASS scores were calculated for all bait-prey interactions, including those involving only mitochondrial prey (gray) and those determined a priori to be high-confidence PPIs based on the literature (black). At each score threshold, the percent of remaining PPI per bin was calculated. Scores to the right of the vertical gray bar exceeded the threshold set for this study and are counted as high-confidence interactions.

(B) Quantitative scoring enriches for high-confidence interactors. (Top) Schematic of the results of CompPASS score filtering. (Bottom left) Heatmap where white indicates a prey was not observed, and shades of gray indicate quantified abundance. Prey proteins are in rows, and FLAG-tagged baits are in columns. Data are averages from six replicates per cell line (three glucose, three galactose). (Bottom right) Heatmap showing scores above CompPASS threshold. Preys and baits are organized in the same order as in left heatmap. Black indicates a score above the threshold. LFQ, label free quantification intensity.

(C) Venn diagram of high-confidence PPIs from each cell line. Mitochondrial interactions above threshold in HEK293 (blue) and HepG2 (green) cells are indicated (see Figure S2).

(D) Venn diagram of high-confidence PPIs from each carbon source. Mitochondrial interactions above threshold in glucose (orange) and galactose (purple) cells are indicated.

(E) Histogram of the fold change abundances of PPIs between carbon sources. Select dynamic PPIs involving proteins from the coenzyme Q biosynthetic pathway (see Figure S6) are indicated.

cDNA. Nonetheless, based on its key role in CI function and its interaction with NDUFAF5 (Figure 4D), we propose to rename *C17orf89* as *NDUFAF8*, and suggest that it is a candidate gene for human CI deficiency.

LYRM5 Binds and Deflavinates the Electron Transferring Flavoprotein

A second MXP that our AE-MS analyses connected to the respiratory chain is LYRM5, an 11 kDa member of the mitochondrial family of LYR motif-containing (LYRM) proteins, which also

include MXPs LYRM1, LYRM2, and LYRM9. LYRM proteins were first identified as supernumerary subunits of CI (NDUFA6 and NDUFB9) and have recently been found to act as assembly factors for CII (SDHAF1/LYRM8, SDHAF3/ACN9) (Atkinson et al., 2011; Ghezzi et al., 2009; Sánchez et al., 2013), CV (FMC1) (LeFebvre-Legendre et al., 2001), and iron-sulfur cluster biosynthetic enzymes (ISD11/LYRM4) (Adam et al., 2006; Shan et al., 2007). Our data capture many of these expected LYRM interactions (Figure 5A). Interestingly, all seven LYRM proteins in our study were found to interact with NDUFAF1, a poorly characterized

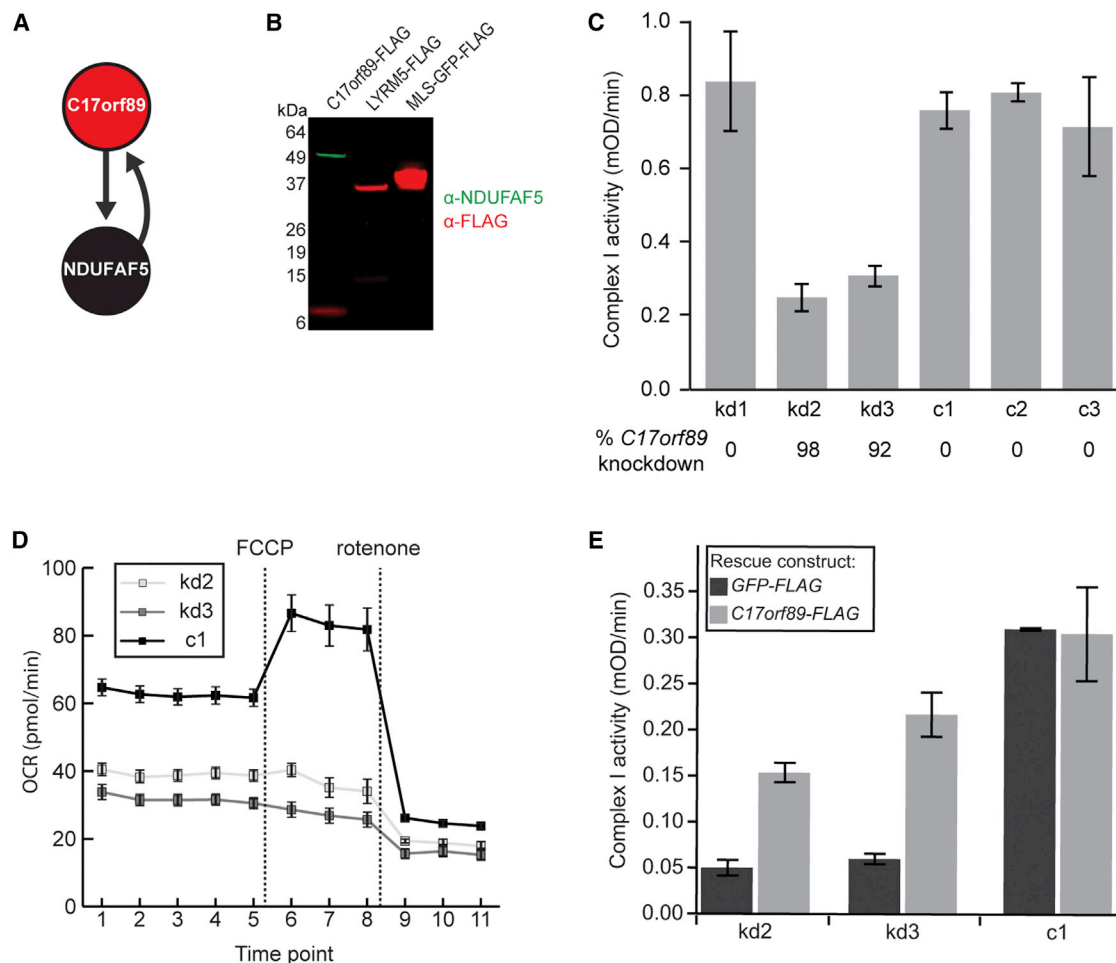


Figure 3. C17orf89 Is Required for Complex I Assembly

(A) Schematic of top-scoring C17orf89 interactions. Arrows originate from bait proteins and point to high-confidence interactors.

(B) Immunoblot of immunoprecipitated FLAG-tagged C17orf89, LYRM5, and MLS-GFP with anti-NDUF5 (green) or anti-FLAG (red).

(C) Activity of complex I in C17orf89 knockdown (kd) and control (c) HEK293 cell lines and control lines. Error bars indicate \pm SD (see also Figure S3). Percent reduction in C17orf89 mRNA is indicated for each cell line.

(D) Measurement of oxygen consumption rate (OCR) for the same kd or c lines as in (C) using a Seahorse Extracellular Flux Analyzer (FCCP, carbonyl cyanide *p*-trifluoromethoxyphenylhydrazone). Error bars indicate \pm SEM.

(E) Complex I activity in kd and c cell lines after transfection with GFP-FLAG (negative control) or C17orf89-FLAG (rescue). Error bars indicate \pm SD.

CI subunit that also serves as an acyl carrier protein (Angerer et al., 2014) (Figure 5A).

Unlike the other LYRM proteins, LYRM5 interacted robustly with ETF and ETFB, which comprise the electron transfer flavoprotein (ETF) (Figure 5A). ETF partners with ETF dehydrogenase to shuttle electrons to CoQ. Notably, LYRM5-FLAG immunoprecipitation enriched for endogenous ETF and ETFB to a much greater extent than does IVD—a known ETF substrate (Kim and Miura, 2004) (Figures 5B and S5). Furthermore, the LYRM5 IP elution generated a single band containing LYRM5, ETF, and ETFB on a BN-PAGE immunoblot (Figure 5C). To test whether the LYRM5-ETF interaction is direct, we purified recombinant ETF and LYRM5 from *E. coli* (Figure 5D) and demonstrated that they form a stable complex by size-exclusion chromatography (Figure 5E). LYRM5 alone eluted as a broad peak around 44 kDa, indicating that it may exist as a tetramer.

Surprisingly, the purified LYRM5-ETF complex lacked the characteristic yellow color of flavoproteins, suggesting that LYRM5 either prevents the incorporation of flavin adenine dinucleotide (FAD) into ETF or that it is capable of removing this cofactor. To test the ability of LYRM5 to “deflavinize” the ETF complex, we mixed LYRM5 and ETF at increasing ratios and measured ETF activity. The addition of LYRM5 led to a linear reduction of ETF activity up to a ratio of 4:1, at which point ETF lost all activity (Figure 6A). This decrease in activity was concomitant with a proportional release of FAD from the ETF complex, as observed by fluorescence emission spectroscopy (Figure 6B). The interaction of FAD with ETF protein residues can be seen by the 420 nm and 460 nm peaks on an absorbance spectrum. These peaks disappear upon addition of LYRM5 (Figure 6C), lending further evidence of its direct deflavination activity. Collectively, these experiments support a direct, specific

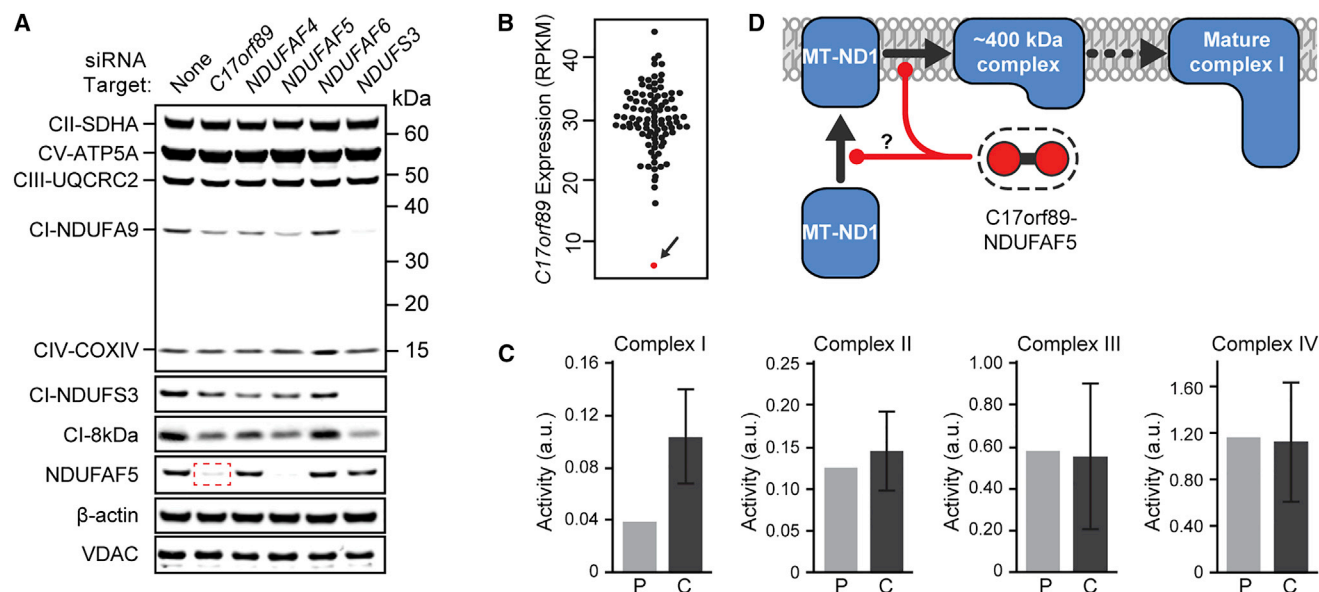


Figure 4. C17orf89 Stabilizes NDUFAF5 and Is Depleted in a Case of CI Deficiency

(A) Immunoblots of mitochondrial proteins in cells treated with siRNA for CI and CIAF genes. C17orf89 knockdown results in loss of CI subunits and a marked depletion of NDUFAF5 (red box). See also Figure S4.

(B) RNaseq analysis of C17orf89 expression in 96 cell lines from patients with respiratory chain dysfunction (RPKM, reads per kilobase of transcript per million mapped reads). Arrow indicates a line with severe loss of C17orf89 expression.

(C) Respiratory chain complex analyses of the patient line indicated in (B), revealing an isolated CI deficiency (P, patient; C, control). Error bars represent mean \pm SD, $n = 25$.

(D) Proposed model of C17orf89-NDUFAF5 complex function in CI assembly.

interaction between LYRM5 and ETF that results in deflavination (Figure 6D)—a unique and unexpected activity that perhaps suggests a non-electron transferring role for ETF (see Discussion).

CoQ Is Synthesized by a Dynamic Biosynthetic Complex

Both CI and ETF operate by shuttling electrons to CoQ—a requisite gateway for electron transport along the mitochondrial respiratory chain. CoQ is synthesized within the mitochondrion in a process that involves at least 13 human proteins, six of which we consider MXPs as they lack well established biochemical roles in the pathway (Figure S6A). Across a series of isolated studies, seven *S. cerevisiae* CoQ proteins, Coq3p–Coq9p, have been found to physically interact and to potentially form a biosynthetic complex (He et al., 2014; Marbois et al., 2005). We and others have speculated that a CoQ complex might exist in other species; however, species-specific aspects of CoQ biosynthesis exist, and, to date, there are only four known human CoQ-related PPIs (Ashraf et al., 2013; Lohman et al., 2014; Nguyen et al., 2014).

Our AE-MS data have now established direct evidence of a highly interconnected mammalian CoQ biosynthetic complex, which we call complex Q (Figure 7A). Intriguingly, the abundances of CoQ pathway PPIs involving COQ8A/ADCK3 increased in galactose-treated cells, and those with COQ8B/ADCK4 reciprocally decreased (Figure 7B)—a phenomenon that accompanied a marked elevation of CoQ levels in HepG2 cells (Figure 7C) (note that ADCK3 and ADCK4 are now referred to as COQ8A and COQ8B, respectively—see Stefely et al. [2016], in this issue of *Molecular Cell*). We consider COQ8A

and COQ8B to be MXPs due to their lack of clear biochemical function; however, consistent with these results, we recently revealed that COQ8A is essential for the stability of CoQ proteins in a mouse model of Coq8a deficiency (Stefely et al., 2016), and COQ8B has been shown to interact with COQ6 (Ashraf et al., 2013). These data suggest an important connection between CoQ production and interactions among CoQ biosynthetic complex members and may indicate reciprocal regulation of the activities of the paralogs COQ8A and COQ8B.

We next aimed to reconstruct the CoQ interactions using purified recombinant proteins. This is a powerful means to validate our observed AE-MS interactions, ascertain the direct interactions between the CoQ proteins, and begin mapping the topology of complex Q. Our in vitro analyses using a cell-free protein translation and purification system revealed that while nearly all COQ proteins were unstable or insoluble when produced alone, many coexpression pairs between COQ3–COQ7 and COQ9 were stabilized by direct interaction (Figures 7D, 7E, and S6B). Strikingly, using this same method, we were then able to rebuild a CoQ complex containing six of the core members in vitro (Figures 7G and 7H). Combined with the binary interactions noted above, these data allow us to propose the subunit topology of the complex (Figures 7F and 7H). While it is likely that other CoQ-related proteins interact with the complex directly or indirectly and are important for its stability in vivo, such as COQ8A and COQ8B, this work suggests that these six core CoQ-related proteins are sufficient to form a complex. These data lend clarity to an evolutionarily conserved complex Q and provide a platform

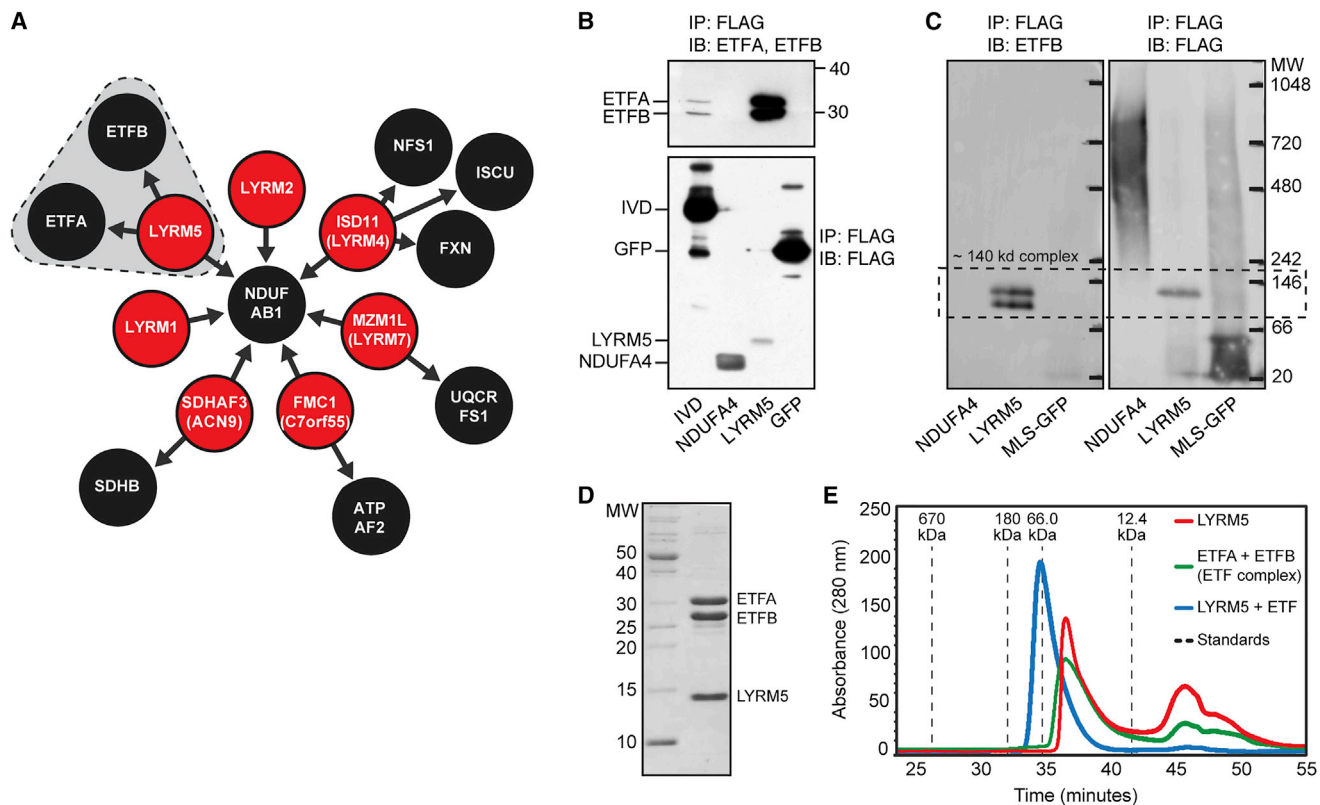


Figure 5. LYRM5 Forms a Complex with ETF

(A) Schematic of top-scoring LYRM PPIs. LYRM5-ETF interactions are shaded.
 (B) Validation of the interaction between LYRM5 and both ETFB and ETFB. C-terminally FLAG-tagged GFP, IVD, NDUF4, and LYRM5 were immunoprecipitated (IP) from HEK cells and immunoblotted (IB) with anti-ETF and anti-ETFB (upper) or anti-FLAG (lower). LYRM5 enriched for both ETF proteins more efficiently than IVD, a known ETF interactor.
 (C) IP of LYRM5-FLAG or MLS-GFP from HEK293 cells analyzed by blue native PAGE analysis and IB. The same membrane was blotted for ETFB (left) and then FLAG (right) (see also Figure S5).
 (D) Recombinant N-terminally His-tagged LYRM5 and untagged ETFB were coexpressed in *E. coli*. Purification of LYRM5 by metal affinity chromatography led to the copurification of ETFB.
 (E) LYRM5 and ETF form a stable complex. Size-exclusion chromatography of LYRM5 alone (red), ETF alone (green), or the co-purified LYRM5-ETF complex (blue) noted in (D).

for the future interrogation of the roles of each complex subunit, including the MXPs COQ4 and COQ9.

Associating MXPs with Other Established Pathways

Our analyses above focused on MXPs related to CI and CoQ in order to build upon our recent work in these areas (Khadria et al., 2014; Lohman et al., 2014; Stefely et al., 2015). However, our data reveal many other connections between MXPs and diverse mitochondrial processes. For instance, C15orf48 also interacts with multiple subunits of CI and CIV (Figure S7), suggesting that it regulates the activity of one or both of these complexes, or perhaps supercomplex formation. C2orf47 interacts with AFG3L2 and SPG7, the two members of the human m-AAA protease complex that is responsible for the maturation of several membrane-associated proteins and for mitochondrial protein quality processes (Ehse et al., 2009) (Figure S7). As a final example, we observed that DHRS4—a poorly characterized member of the short-chain dehydrogenases/reductases (SDR)

family (Persson and Kallberg, 2013)—interacts with other members of the SDR family, including DHRS4L2 and CBR4, as well as with SIRT3 and EHHADH (Figure S7). DHRS4 is reported to have dual localization to peroxisomes and mitochondria (Matsunaga et al., 2008; Pagliarini et al., 2008) and is dynamically phosphorylated and acetylated (Grimsrud et al., 2012; Still et al., 2013); however, no direct function is known. These interactions suggest that DHRS4 might have an important unappreciated role in coordinating lipid metabolism between these organelles. Our other top-scoring interactions, and many others that fall just below our stringent cutoff, can likewise enable new hypotheses about MXP function (Table S2).

DISCUSSION

Insights into Mitochondrial Respiratory Chain Function

Our identification of C17orf89/NDUF4F8 as a complex I assembly factor (CIAF) pinpoints it as a disease gene candidate for

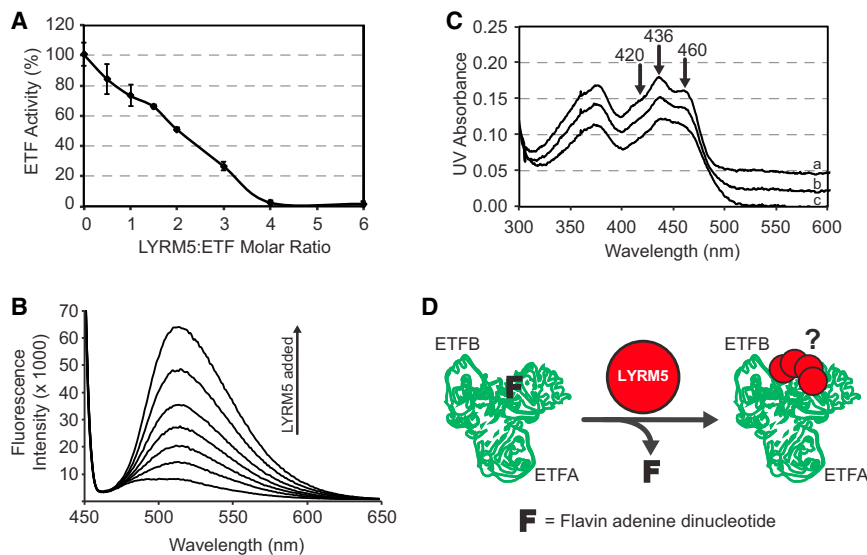


Figure 6. LYRM5 Deflavinates ETF

(A) ETF activity in the presence of increasing amounts of LYRM5 (\pm SD from triplicate measurements).

(B) FAD release from ETF upon incubation with varying amounts of LYRM5, measured by fluorescence emission spectroscopy.

(C) Visible spectra of ETF in the presence of LYRM5. The flavin visible spectrum shows two shoulder peaks at 420 nm and 460 nm due to the interaction between FAD and ETF protein residues that are lost upon addition of LYRM5. Spectra a, b, and c are for LYRM5:ETF ratios of 0, 2, and 4, respectively. For clarity, spectra a and b have been shifted by +0.04 and 0.02 OD units, respectively.

(D) Proposed model of the functional interaction between LYRM5 and ETF. Binding of four molar equivalents of LYRM5 (red dot) to ETF (green trace of PDB ID 1EFV) leads to the loss of FAD from ETF (F).

unresolved cases of isolated CI deficiency. Given the presence of twin CX₉C domains in its primary structure, C17orf89/NDUFAF8 is likely a member of the coiled-coil-helix-coiled-coil-helix (CHCH) domain family of proteins (Modjtahedi et al., 2016). Many CHCH proteins are mitochondrial, and several are involved in respiratory chain functions, including four CI subunits (Modjtahedi et al., 2016). Our data revealed a robust interaction between C17orf89/NDUFAF8 and NDUFAF5—a putative methyltransferase that is essential for early stages of CI assembly (Pagliarini et al., 2008; Sugiana et al., 2008), but for which neither a substrate nor a direct role in CI maturation has been elucidated. Interestingly, several similar sub-complexes of CIAFs exist, including the mitochondrial CI assembly (MCIA) complex (Guarani et al., 2014) and the NDUFAF3:NDUFAF4 complex (Saada et al., 2009). Given that C17orf89/NDUFAF8 interacts with and stabilizes NDUFAF5, we suggest that C17orf89 may facilitate the methyltransferase activity of NDUFAF5, or even be its substrate. Furthermore, as we identified a patient with CI deficiency whose molecular diagnosis eluded whole-genome sequencing but who is deficient in C17orf89/NDUFAF8 transcript, we both prioritize this as a disease gene and highlight the importance of complementary methods for the diagnosis of genetic diseases.

CI is one of several sources of electrons entering the CoQ pool for transport along the respiratory chain. A second source is ETF, which interacts with and accepts electrons from various mitochondrial dehydrogenases before passing them to ETFDH (Roberts et al., 1996). ETF harbors causal mutations in glutaric acidemia type 2 (GA2) (Vockley and Whiteman, 2002), and other cases of GA2 remain unresolved (Schiff et al., 2006). Given this, we were particularly interested in our observed interaction of ETF with LYRM5.

We discovered that the interaction between LYRM5 and ETF results in an efficient—and surprising—removal of FAD from the ETF holoenzyme. Much work needs to be done to understand the *in vivo* utility of this process, but a few possibilities stand out. First, the FAD of ETF could become damaged and need to be replaced. Second, removal of FAD may facilitate

the destabilization of ETF and allow for proteolysis and recycling of the flavin cofactor. Third, if in a given metabolic state ETF is not interacting with dehydrogenases (i.e., its electron transfer partners), its FAD would be free to interact with water or other matrix metabolites and generate reactive oxygen species (Rodrigues and Gomes, 2012). In this scenario, LYRM5 could act to shut down ETF activity without the need to completely turn over the enzyme. Finally, it is possible that ETF possesses a distinct, non-electron transferring function—a possibility we most favor. Consistent with this hypothesis is our observation that LYRM5, like other LYRM proteins (Figure 5A), interacts with the CI subunit NDUFAF1—the mitochondrial acyl carrier protein (ACP) (Angerer, 2015; Angerer et al., 2014). It is possible that LYRM5 serves as an adaptor to bring ETF to CI via NDUFAF1 to perform an unidentified function. Given our functional discoveries, we propose renaming C17orf89 and LYRM5 as *NDUF Assembly Factor 8* (NDUFAF8) and *ETF Regulatory Factor 1* (ETFRF1), respectively.

Insights into CoQ Biosynthesis

CoQ is a requisite gateway in the respiratory chain that accepts electrons from many sources, including CI and ETF (via ETFDH). Although it was discovered 60 years ago, multiple aspects of eukaryotic CoQ biosynthesis remain unexplained, including roles for MXPs COQ8A, COQ8B, COQ4, and COQ9 (Figure S6A).

Two notable features emerged from our work with the CoQ machinery. First, it is abundantly clear that the mammalian CoQ proteins physically interact to form what appears to be a biosynthetic complex—complex Q. *Saccharomyces cerevisiae* is also known to have a partially defined complex, but it is not known how this complex facilitates CoQ biosynthesis. Our work here provides insights into the binary interactions that likely enable the formation of complex Q in both species. Second, our work implicates MXPs ADCK3 and ADCK4 (aka COQ8A and COQ8B, respectively) in complex Q and show that their interactions with the complex are both dynamic and reciprocal. COQ8A and COQ8B are paralogs that are each likely orthologs of yeast

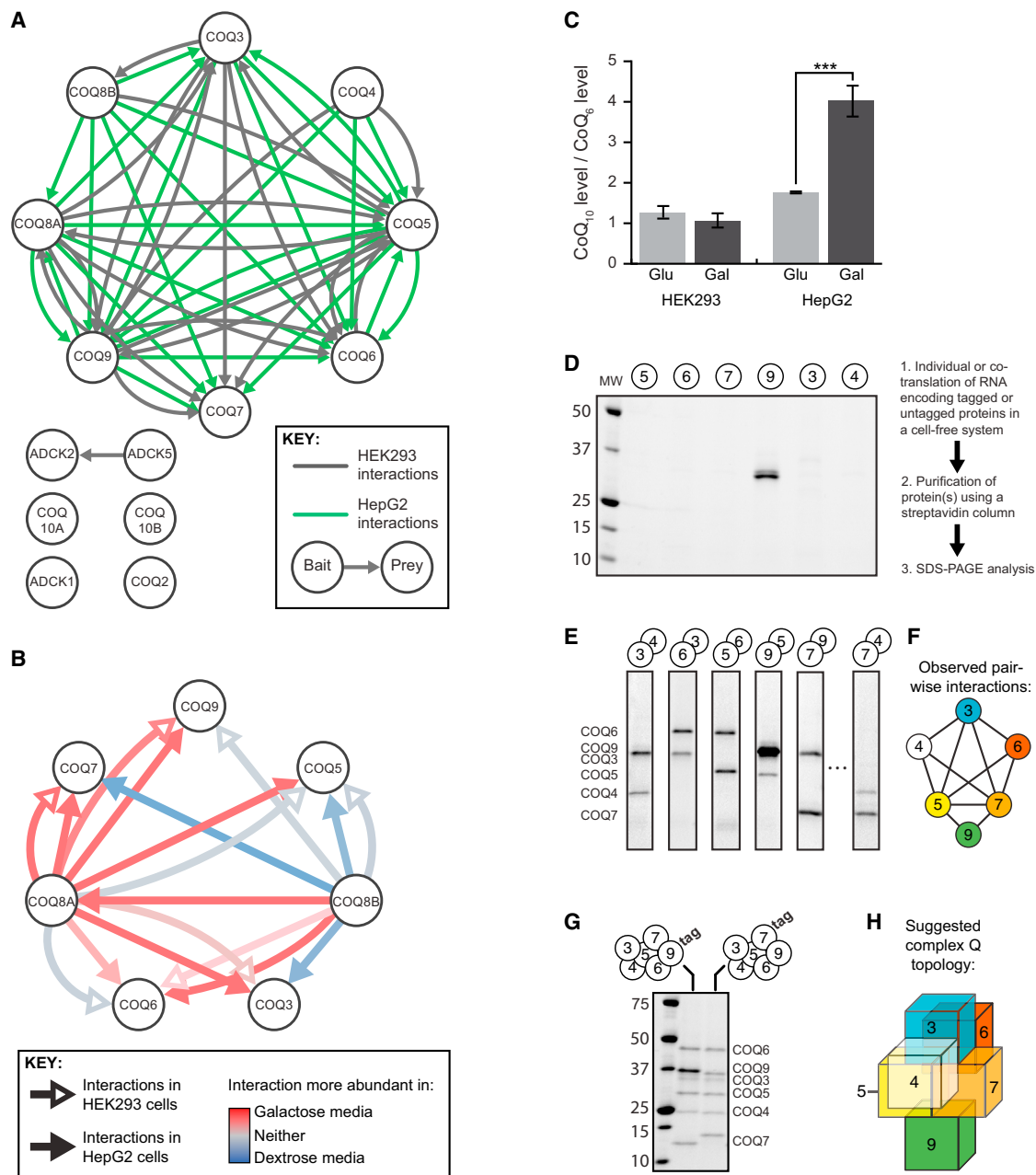


Figure 7. Interaction Analysis Reveals the Dynamic Human CoQ-Related Complex

(A) All CoQ-related proteins used as baits and/or observed as preys in this study are shown as white nodes. Interactions above our score threshold are shown for HEK293 cells (gray arrows) or HepG2 cells (green arrows).

(B) CoQ-related interactions involving COQ8A or COQ8B as bait were assessed for the effect of cellular metabolic status. Interactions more abundant in galactose or glucose media are shown in red or blue, respectively, while those with no clear media effect are in gray. See also [Table S3](#) for primary data.

(C) Relative abundance of CoQ₁₀ in HEK293 and HepG2 cells after treatment with 10 mM glucose or galactose for 24 hr (***) indicates t test $p < 0.001$, error bars indicate the 95% confidence interval).

(D and E) Representative results of in vitro protein translation and purification of each core CoQ complex protein individually (D) or in pairs (E). Proteins were run on SDS-PAGE and detected by Coomassie stain. See [Figure S6](#) for all interactions observed.

(F) Schematic of COQ protein network direct interactions established in vitro. All robust interactions are represented as edges between the COQ protein nodes.

(G) In vitro co-purification of all six core COQ complex proteins. "Tag" indicates sole protein with strep tag II affinity tag.

(H) Three-dimensional model of predicted COQ complex structure based on in vitro interaction data. Colors are as in [Figure 7F](#).

Coq8p, and we have speculated that they possess redundant functions in a condition- or tissue-specific manner. We recently have shown that COQ8A adopts an atypical protein kinase-like fold (Stefely et al., 2015) and, building off of the work here, have now determined that its function is essential for maintaining complex Q stability (Stefely et al., 2016).

Overall, we have extended the annotation of the mammalian mitochondrial proteome by identifying robust PPIs involving MXPs and by validating roles for these proteins in well-characterized mitochondrial pathways. Other prominent PPIs from our study now await further biological investigation, and many more that fell below our stringent cutoff score will nonetheless serve as important clues for the functional annotation of MXPs moving forward (Table S3). As such, our compendium of state-specific MXP associations will continue to serve as a powerful resource for the characterization of mitochondrial proteins, thereby advancing our understanding of basic mitochondrial biology and its associated pathophysiology.

EXPERIMENTAL PROCEDURES

Mitochondrial Proteome Compilation

Entrez GeneIDs of the mouse MitoCarta (Pagliarini et al., 2008) were converted from mouse to human using HomoloGene and reciprocal BLASTP searches. Data from the mitochondrial matrix (Rhee et al., 2013), inter-membrane space (Hung et al., 2014) proteomic studies, and other high-quality studies were then integrated with the human MitoCarta 2.0 (Calvo et al., 2016) to generate our MitoCarta+ list of mitochondrial proteins.

Generation of Tagged Constructs

Mitochondrial open reading frames were obtained from The Broad Institute and DNASU (Seiler et al., 2014) and cloned into a pcDNA3.1 mammalian expression vector with a C-terminal FLAG tag.

Mammalian Cell Culture

HEK293 or HepG2 cells were transiently transfected with pcDNA3.1 gene-FLAG plasmids using linear polyethylenimine (PEI, PolySciences) and Opti-MEM (LifeTechnologies). After 48 hr, cells were washed with PBS, and media was replaced with DMEM containing either 10 mM glucose or 10 mM galactose. After 24 hr, cells were washed with and harvested into phosphate-buffered saline (PBS), snap frozen in liquid nitrogen, and stored at -80°C .

Affinity Enrichment

Cell pellets were lysed in 200 μl buffer (see Supplemental Experimental Procedures). After vortexing on ice, insoluble materials were pelleted (16,000 g, 10 min, 4°C). Equal masses of cell supernatant were mixed with 30 μl pre-washed anti-FLAG magnetic beads (Sigma M8823) for 2–3 hr at 4°C with end-over-end agitation. Following incubation, beads were washed four times and proteins were eluted in 70 μl elution buffer containing 0.2 mg/mL FLAG-peptide for 30 min at room temperature with constant agitation.

LC-MS/MS Analysis

All experiments were performed using a NanoAcquity UPLC system (Waters, Milford, MA) coupled to an Orbitrap Elite mass spectrometer (Thermo Fisher Scientific, San Jose, CA). Reverse-phase columns were made in house by packing a fused silica capillary with 3.5 μm diameter, 130 Å pore size Bridged Ethylene Hybrid C18 particles (Waters) to a final length of 30 cm. The column was heated to 55°C for all experiments. Precursor trypsin-digested peptide cations were generated from the eluent through the utilization of a nanoESI source. MS instrument methods consisted of MS¹ survey scans that were used to guide 15 subsequent data-dependent MS/MS scans. Raw data can be found on Chorus (<https://chorusproject.org>) under project ID 1043.

Data Analysis

Data were processed using the MaxQuant software suite (Cox and Mann, 2008; Cox et al., 2011). Searches were performed against a target-decoy database using the default settings for high-resolution mass spectra. Results were filtered to 1% FDR at the unique peptide level and grouped into proteins within MaxQuant. Proteins were quantified across all replicates within each bait set using MaxLFQ (Cox et al., 2014).

Generation of C17orf89 Knockdown Cells

Viral particles were produced in HEK293 cells by transient transfection with PEI of lentiviral shRNA construct, psPAX2, and pMD2.G packaging plasmids. HEK293 cells were transduced in 6-well plates and were selected in culture medium supplemented with 2 $\mu\text{g}/\text{ml}$ puromycin for at least 2 weeks. For siRNA knockdowns, HEK293 cells were transfected with 10 nM RNA for each target or the non-targeting siRNA based on the manufacturer's protocol. After 2 days, the cells were passaged; the next day were transfected again with 10 nM siRNA; and after another 2 days were collected for real-time qPCR, immunoblot, and MS-based proteomic analyses.

CI Activity and C17orf89 Sequencing and Expression Analysis

Patients with biochemical evidence of isolated complex I deficiency identified via diagnostic work-up for suspected mitochondrial disease were screened for disruptive variants in C17orf89 by Sanger sequencing (primers available on request). C17orf89 transcript abundance in control and patient lines was measured as described previously (Haack et al., 2015). Informed consent for diagnostic and research studies was obtained in accordance with the Declaration of Helsinki protocols and approved by local Institutional Review Boards.

Purification and Functional Analyses of LYRM5 and ETF

LYRM5 was cloned into a pET28a vector and purified as an N-terminally His-tagged protein by immobilized metal affinity chromatography. Size-exclusion chromatography was performed using a Pharmacia 300 \times 10 mm Superdex 200 column. ETF activity \pm LYRM5 was measured by monitoring DCPIP reduction at 600 nm. For assay conditions, 40 μM DCPIP, 20 μM C₈-CoA, and 0.1–0.2 μM ETF were mixed in 20 mM Tris-HCl buffer (pH 8.0). The assay reactions were initiated by adding 0.2 μM MCAD, and the UV absorbance decrease at 600 nm was followed for 3 min. FAD release was measured by first mixing 10 μM ETF with varying amounts of LYRM5 and incubated on ice for 2 hr. The samples were then diluted five times in 20 mM Tris-HCl buffer (pH 8.0), and the fluorescence emission spectra were taken at room temperature (λ_{ex} = 436 nm). Visible spectra measurements of 10 μM ETF were measured in the presence of 0, 20, and 40 μM LYRM5 in 20 mM Tris-HCl buffer (pH 8.0).

Blue Native PAGE

Samples were mixed with native PAGE sample buffer to 1 \times final concentration and were loaded onto native PAGE gels alongside native MARK standard. Gels were run for a total of 2 hr and subsequently subjected to western analysis.

Coenzyme Q Quantification

Tissue culture cells were lysed by vortexing with glass beads and spiked with an internal standard (CoQ₉). Lipids were extracted with CHCl₃/MeOH (1:1, v/v) and analyzed by LC-MS/MS.

Cell-free Expression and Purification

Purified plasmid DNA was used as individual transcription templates with SP6 RNase polymerase. Transcription and translation methods are as previously described (Makino et al., 2013).

SUPPLEMENTAL INFORMATION

Supplemental Information includes seven figures, three tables, and Supplemental Experimental Procedures and can be found with this article at <http://dx.doi.org/10.1016/j.molcel.2016.06.033>.

AUTHOR CONTRIBUTIONS

B.J.F. and D.J.P. conceived of the project and its design. B.J.F., C.E.M., E.M.W., M.T.V., C.X., E.T.B., H.C., L.S.K., C.L.A., K.A.G., B.K.D., A.U., J.A.S., S.L.B., K.M.W., J.W.R., R.W.T., H.P., J.J.K., J.J.C., and D.J.P. performed experiments and data analysis. R.L.W., A.J., M.S.W., J.W.R., R.W.T., H.P., J.J.K., J.J.C., and D.J.P. provided key experimental resources and/or aided in experimental design. B.J.F. and D.J.P. wrote the manuscript.

ACKNOWLEDGMENTS

We thank David Aceti, John Primm, Brian Fox, and John Markley for technical and managerial assistance and Clay Williams for MS technical support. This work was supported by a Searle Scholars Award and NIH grants U01GM94622, R01DK098672, R01GM112057, and R01GM115591 (to D.J.P.); R35GM118110 (to J.J.C.); R01GM029076 (to J.-J.P.K.); T32DK007665 and T32GM008692 MSTP (to B.J.F.); T15LM007359 (to C.E.M.); T32HL007899 (to E.M.W.); F30AG043282 (to J.A.S.); and T32GM07215 (to K.M.W.); and also by a Wisconsin Distinguished Graduate Fellowship (to B.J.F.) and an NSF Graduate Research Fellowship (to M.T.V.). R.W.T. is funded by a Wellcome Trust Strategic Award (096919/Z/11/Z), MRC Centre for Neuromuscular Diseases (G0601943), UK NHS Highly Specialised “Rare Mitochondrial Disorders of Adults and Children” Service, and The Lily Foundation. C.L.A. is the recipient of a National Institute for Health Research (NIHR) doctoral fellowship (NIHR-HCS-D12-03-04). H.P. was supported by the German Bundesministerium für Bildung und Forschung (BMBF) through the German Network for mitochondrial disorders (mitoNET, 01GM1113C) and the E-Rare project GENOMIT (01GM1603), the EC FP7-PEOPLE-ITN Mitochondrial European Educational Training Project (GA #317433) and EU Horizon2020 Collaborative Research Project SOUND (633974).

Received: June 30, 2015

Revised: March 25, 2016

Accepted: June 21, 2016

Published: August 4, 2016

REFERENCES

Adam, A.C., Bornhövd, C., Prokisch, H., Neupert, W., and Hell, K. (2006). The Nfs1 interacting protein Isp1 has an essential role in Fe/S cluster biogenesis in mitochondria. *EMBO J.* 25, 174–183.

Angerer, H. (2015). Eukaryotic LYR Proteins Interact with Mitochondrial Protein Complexes. *Biology (Basel)* 4, 133–150.

Angerer, H., Radermacher, M., Mańkowska, M., Steger, M., Zwicker, K., Heide, H., Wittig, I., Brandt, U., and Zickermann, V. (2014). The LYR protein subunit NB4M/NDUFA6 of mitochondrial complex I anchors an acyl carrier protein and is essential for catalytic activity. *Proc. Natl. Acad. Sci. USA* 111, 5207–5212.

Ashraf, S., Gee, H.Y., Woerner, S., Xie, L.X., Vega-Warner, V., Lovric, S., Fang, H., Song, X., Catttran, D.C., Avila-Casado, C., et al. (2013). ADCK4 mutations promote steroid-resistant nephrotic syndrome through CoQ10 biosynthesis disruption. *J. Clin. Invest.* 123, 5179–5189.

Atkinson, A., Smith, P., Fox, J.L., Cui, T.-Z., Khalimonchuk, O., and Winge, D.R. (2011). The LYR protein Mzm1 functions in the insertion of the Rieske Fe/S protein in yeast mitochondria. *Mol. Cell. Biol.* 31, 3988–3996.

Calvo, S.E., Tucker, E.J., Compton, A.G., Kirby, D.M., Crawford, G., Burt, N.P., Rivas, M., Guiducci, C., Bruno, D.L., Goldberger, O.A., et al. (2010). High-throughput, pooled sequencing identifies mutations in NUBPL and FOXRED1 in human complex I deficiency. *Nat. Genet.* 42, 851–858.

Calvo, S.E., Clauser, K.R., and Mootha, V.K. (2016). MitoCarta2.0: an updated inventory of mammalian mitochondrial proteins. *Nucleic Acids Res.* 44 (D1), D1251–D1257.

Cox, J., and Mann, M. (2008). MaxQuant enables high peptide identification rates, individualized p.p.b.-range mass accuracies and proteome-wide protein quantification. *Nat. Biotechnol.* 26, 1367–1372.

Cox, J., Neuhauser, N., Michalski, A., Scheltema, R.A., Olsen, J.V., and Mann, M. (2011). Andromeda: a peptide search engine integrated into the MaxQuant environment. *J. Proteome Res.* 10, 1794–1805.

Cox, J., Hein, M.Y., Lubner, C.A., Paron, I., Nagaraj, N., and Mann, M. (2014). Accurate proteome-wide label-free quantification by delayed normalization and maximal peptide ratio extraction, termed MaxLFQ. *Mol. Cell. Proteomics* 13, 2513–2526.

Ehse, S., Raschke, I., Mancuso, G., Bernacchia, A., Geimer, S., Tondera, D., Martinou, J.-C., Westermann, B., Rugari, E.I., and Langer, T. (2009). Regulation of OPA1 processing and mitochondrial fusion by m-AAA protease isoenzymes and OMA1. *J. Cell Biol.* 187, 1023–1036.

Fernández-Vizcarra, E., and Zeviani, M. (2015). Nuclear gene mutations as the cause of mitochondrial complex III deficiency. *Front. Genet.* 6, 134.

Ghezzi, D., Goffrini, P., Uziel, G., Horvath, R., Klopstock, T., Lochmüller, H., D’Adamo, P., Gasparini, P., Strom, T.M., Prokisch, H., et al. (2009). SDHAF1, encoding a LYR complex-II specific assembly factor, is mutated in SDH-defective infantile leukoencephalopathy. *Nat. Genet.* 41, 654–656.

Grimsrud, P.A., Carson, J.J., Hebert, A.S., Hubler, S.L., Niemi, N.M., Bailey, D.J., Jochem, A., Stapleton, D.S., Keller, M.P., Westphall, M.S., et al. (2012). A quantitative map of the liver mitochondrial phosphoproteome reveals post-translational control of ketogenesis. *Cell Metab.* 16, 672–683.

Guarani, V., Paulo, J., Zhai, B., Huttlin, E.L., Gygi, S.P., and Harper, J.W. (2014). TIMMDC1/C3orf1 functions as a membrane-embedded mitochondrial complex I assembly factor through association with the MCIA complex. *Mol. Cell. Biol.* 34, 847–861.

Haack, T.B., Madignier, F., Herzer, M., Lamantea, E., Danhauser, K., Invernizzi, F., Koch, J., Freitag, M., Drost, R., Hillier, I., et al. (2011). Mutation screening of 75 candidate genes in 152 complex I deficiency cases identifies pathogenic variants in 16 genes including NDUFB9. *J. Med. Genet.* 49, 83–89.

Haack, T.B., Stauffer, C., Köpke, M.G., Straub, B.K., Köler, S., Thiel, C., Freisinger, P., Baric, I., McKiernan, P.J., Dikow, N., et al. (2015). Biallelic mutations in NBAS cause recurrent acute liver failure with onset in infancy. *Am. J. Hum. Genet.* 97, 163–169.

He, C.H., Xie, L.X., Allan, C.M., Tran, U.C., and Clarke, C.F. (2014). Coenzyme Q supplementation or over-expression of the yeast Coq8 putative kinase stabilizes multi-subunit Coq polypeptide complexes in yeast coq null mutants. *Biochim. Biophys. Acta* 1841, 630–644.

Hein, M.Y., Hubner, N.C., Poser, I., Cox, J., Nagaraj, N., Toyoda, Y., Gak, I.A., Weisswange, I., Mansfeld, J., Buchholz, F., et al. (2015). A human interactome in three quantitative dimensions organized by stoichiometries and abundances. *Cell* 163, 712–723.

Hosp, F., Scheltema, R.A., Eberl, H.C., Kulak, N.A., Keilhauer, E.C., Mayr, K., and Mann, M. (2015). A double-barrel liquid chromatography-tandem mass spectrometry (LC-MS/MS) system to quantify 96 interactomes per day. *Mol. Cell. Proteomics* 14, 2030–2041.

Hung, V., Zou, P., Rhee, H.-W., Udeshi, N.D., Cracan, V., Svinkina, T., Carr, S.A., Mootha, V.K., and Ting, A.Y. (2014). Proteomic mapping of the human mitochondrial intermembrane space in live cells via ratiometric APEX tagging. *Mol. Cell* 55, 332–341.

Huttlin, E.L., Ting, L., Bruckner, R.J., Gebreab, F., Gygi, M.P., Szpyt, J., Tam, S., Zarraga, G., Colby, G., Baltier, K., et al. (2015). The BioPlex Network: a systematic exploration of the human interactome. *Cell* 162, 425–440.

Jäger, S., Cimermancic, P., Gulbahce, N., Johnson, J.R., McGovern, K.E., Clarke, S.C., Shales, M., Mercenne, G., Pache, L., Li, K., et al. (2012). Global landscape of HIV-human protein complexes. *Nature* 481, 365–370.

Jain-Ghai, S., Cameron, J.M., Al Maawali, A., Blaser, S., MacKay, N., Robinson, B., and Raiman, J. (2013). Complex II deficiency—a case report and review of the literature. *Am. J. Med. Genet. A* 161A, 285–294.

Keilhauer, E.C., Hein, M.Y., and Mann, M. (2015). Accurate protein complex retrieval by affinity enrichment mass spectrometry (AE-MS) rather than affinity purification mass spectrometry (AP-MS). *Mol. Cell. Proteomics* 14, 120–135.

Khadria, A.S., Mueller, B.K., Stefely, J.A., Tan, C.H., Pagliarini, D.J., and Senes, A. (2014). A Gly-zipper motif mediates homodimerization of the

- p>transmembrane domain of the mitochondrial kinase ADCK3.
- J. Am. Chem. Soc.*
- 136**
- , 14068–14077.
- Kim, J.J., and Miura, R. (2004). Acyl-CoA dehydrogenases and acyl-CoA oxidases. Structural basis for mechanistic similarities and differences. *Eur. J. Biochem.* **271**, 483–493.
- Kirby, D.M., Thorburn, D.R., Turnbull, D.M., and Taylor, R.W. (2007). Biochemical assays of respiratory chain complex activity. *Methods Cell Biol.* **80**, 93–119.
- Koopman, W.J.H., Willems, P.H.G.M., and Smeitink, J.A.M. (2012). Monogenic mitochondrial disorders. *N. Engl. J. Med.* **366**, 1132–1141.
- Lefebvre-Legendre, L., Vaillier, J., Benabdelhak, H., Velours, J., Slonimski, P.P., and di Rago, J.P. (2001). Identification of a nuclear gene (FMC1) required for the assembly/stability of yeast mitochondrial F(1)-ATPase in heat stress conditions. *J. Biol. Chem.* **276**, 6789–6796.
- Lohman, D.C., Forouhar, F., Beebe, E.T., Stefely, M.S., Minogue, C.E., Ulbrich, A., Stefely, J.A., Sukumar, S., Luna-Sánchez, M., Jochem, A., et al. (2014). Mitochondrial COQ9 is a lipid-binding protein that associates with COQ7 to enable coenzyme Q biosynthesis. *Proc. Natl. Acad. Sci. USA* **111**, E4697–E4705.
- Makino, S.-i., Beebe, E.T., Markley, J.L., and Fox, B.G. (2013). Cell-Free Protein Synthesis for Functional and Structural Studies (Totowa, N.J.: Humana Press), pp. 161–178.
- Marbois, B., Gin, P., Faull, K.F., Poon, W.W., Lee, P.T., Strahan, J., Shepherd, J.N., and Clarke, C.F. (2005). Coq3 and Coq4 define a polypeptide complex in yeast mitochondria for the biosynthesis of coenzyme Q. *J. Biol. Chem.* **280**, 20231–20238.
- Matsunaga, T., Endo, S., Maeda, S., Ishikura, S., Tajima, K., Tanaka, N., Nakamura, K.T., Imamura, Y., and Hara, A. (2008). Characterization of human DHRS4: an inducible short-chain dehydrogenase/reductase enzyme with 3 β -hydroxysteroid dehydrogenase activity. *Arch. Biochem. Biophys.* **477**, 339–347.
- Modjtahedi, N., Tokatlidis, K., Dessen, P., and Kroemer, G. (2016). Mitochondrial proteins containing coiled-coil-helix-coiled-coil-helix (CHCH) domains in health and disease. *Trends Biochem. Sci.* **41**, 245–260.
- Nguyen, T.P.T., Casarin, A., Desbats, M.A., Doimo, M., Trevisson, E., Santos-Ocaña, C., Navas, P., Clarke, C.F., and Salviati, L. (2014). Molecular characterization of the human COQ5 C-methyltransferase in coenzyme Q10 biosynthesis. *Biochim. Biophys. Acta* **1841**, 1628–1638.
- Nunnari, J., and Suomalainen, A. (2012). Mitochondria: in sickness and in health. *Cell* **148**, 1145–1159.
- Pagliarini, D.J., and Rutter, J. (2013). Hallmarks of a new era in mitochondrial biochemistry. *Genes Dev.* **27**, 2615–2627.
- Pagliarini, D.J., Calvo, S.E., Chang, B., Sheth, S.A., Vafai, S.B., Ong, S.E., Walford, G.A., Sugiana, C., Boneh, A., Chen, W.K., et al. (2008). A mitochondrial protein compendium elucidates complex I disease biology. *Cell* **134**, 112–123.
- Persson, B., and Kallberg, Y. (2013). Classification and nomenclature of the superfamily of short-chain dehydrogenases/reductases (SDRs). *Chem. Biol. Interact.* **202**, 111–115.
- Rhee, H.-W., Zou, P., Udeshi, N.D., Martell, J.D., Mootha, V.K., Carr, S.A., and Ting, A.Y. (2013). Proteomic mapping of mitochondria in living cells via spatially restricted enzymatic tagging. *Science* **339**, 1328–1331.
- Roberts, D.L., Frerman, F.E., and Kim, J.J. (1996). Three-dimensional structure of human electron transfer flavoprotein to 2.1-Å resolution. *Proc. Natl. Acad. Sci. USA* **93**, 14355–14360.
- Rodrigues, J.V., and Gomes, C.M. (2012). Mechanism of superoxide and hydrogen peroxide generation by human electron-transfer flavoprotein and pathological variants. *Free Radic. Biol. Med.* **53**, 12–19.
- Saada, A., Vogel, R.O., Hoefs, S.J., van den Brand, M.A., Wessels, H.J., Willems, P.H., Venselaar, H., Shaag, A., Barghuti, F., Reish, O., et al. (2009). Mutations in NDUFAF3 (C3ORF60), encoding an NDUFAF4 (C6ORF66)-interacting complex I assembly protein, cause fatal neonatal mitochondrial disease. *Am. J. Hum. Genet.* **84**, 718–727.
- Saada, A., Edvardson, S., Shaag, A., Chung, W.K., Segel, R., Miller, C., Jalas, C., and Elpeleg, O. (2012). Combined OXPHOS complex I and IV defect, due to mutated complex I assembly factor C20ORF7. *J. Inher. Metab. Dis.* **35**, 125–131.
- Sahni, N., Yi, S., Taipale, M., Fuxman Bass, J.I., Coulombe-Huntington, J., Yang, F., Peng, J., Weile, J., Karras, G.I., Wang, Y., et al. (2015). Widespread macromolecular interaction perturbations in human genetic disorders. *Cell* **161**, 647–660.
- Sánchez, E., Lobo, T., Fox, J.L., Zeviani, M., Winge, D.R., and Fernández-Vizarra, E. (2013). LYRM7/MZM1L is a UQCRCF1 chaperone involved in the last steps of mitochondrial Complex III assembly in human cells. *Biochim. Biophys. Acta* **1827**, 285–293.
- Schiff, M., Froissart, R., Olsen, R.K., Acquaviva, C., and Vianey-Saban, C. (2006). Electron transfer flavoprotein deficiency: functional and molecular aspects. *Mol. Genet. Metab.* **88**, 153–158.
- Seiler, C.Y., Park, J.G., Sharma, A., Hunter, P., Surapaneni, P., Sedillo, C., Field, J., Algar, R., Price, A., Steel, J., et al. (2014). DNASU plasmid and PSI: Biology-Materials repositories: resources to accelerate biological research. *Nucleic Acids Res.* **42**, D1253–D1260.
- Shan, Y., Napoli, E., and Cortopassi, G. (2007). Mitochondrial frataxin interacts with ISD11 of the NFS1/ISCU complex and multiple mitochondrial chaperones. *Hum. Mol. Genet.* **16**, 929–941.
- Sowa, M.E., Bennett, E.J., Gygi, S.P., and Harper, J.W. (2009). Defining the human deubiquitinating enzyme interaction landscape. *Cell* **138**, 389–403.
- Stefely, J.A., Reidenbach, A.G., Ulbrich, A., Oruganty, K., Floyd, B.J., Jochem, A., Saunders, J.M., Johnson, I.E., Minogue, C.E., Wrobel, R.L., et al. (2015). Mitochondrial ADCK3 employs an atypical protein kinase-like fold to enable coenzyme Q biosynthesis. *Mol. Cell* **57**, 83–94.
- Stefely, J.A., Licitra, F., Laredj, L., Reidenbach, A.G., Kemmerer, Z.A., Grangeray, A., Jaeg-Ehret, T., Minogue, C.E., Ulbrich, A., Hutchins, P.D., et al. (2016). Cerebellar ataxia and coenzyme Q deficiency through loss of unorthodox kinase activity. *Mol. Cell* **63**, Published online August 4, 2016. <http://dx.doi.org/10.1016/j.molcel.2016.06.030>.
- Still, A.J., Floyd, B.J., Hebert, A.S., Bingman, C.A., Carson, J.J., Gunderson, D.R., Dolan, B.K., Grimsrud, P.A., Dittenhafer-Reed, K.E., Stapleton, D.S., et al. (2013). Quantification of mitochondrial acetylation dynamics highlights prominent sites of metabolic regulation. *J. Biol. Chem.* **288**, 26209–26219.
- Sugiana, C., Pagliarini, D.J., McKenzie, M., Kirby, D.M., Salemi, R., Abu-Amero, K.K., Dahl, H.H., Hutchison, W.M., Vascotto, K.A., Smith, S.M., et al. (2008). Mutation of C20orf7 disrupts complex I assembly and causes lethal neonatal mitochondrial disease. *Am. J. Hum. Genet.* **83**, 468–478.
- Vockley, J., and Whiteman, D.A. (2002). Defects of mitochondrial beta-oxidation: a growing group of disorders. *Neuromuscul. Disord.* **12**, 235–246.

Supplemental Information

Mitochondrial Protein Interaction

Mapping Identifies Regulators

of Respiratory Chain Function

Brendan J. Floyd, Emily M. Wilkerson, Mike T. Veling, Catie E. Minogue, Chuanwu Xia, Emily T. Beebe, Russell L. Wrobel, Holly Cho, Laura S. Kremer, Charlotte L. Alston, Katarzyna A. Gromek, Brendan K. Dolan, Arne Ulbrich, Jonathan A. Stefely, Sarah L. Bohl, Kelly M. Werner, Adam Jochem, Michael S. Westphall, Jarred W. Rensvold, Robert W. Taylor, Holger Prokisch, Jung-Ja P. Kim, Joshua J. Coon, and David J. Pagliarini

Figure S1, related to Figure 1

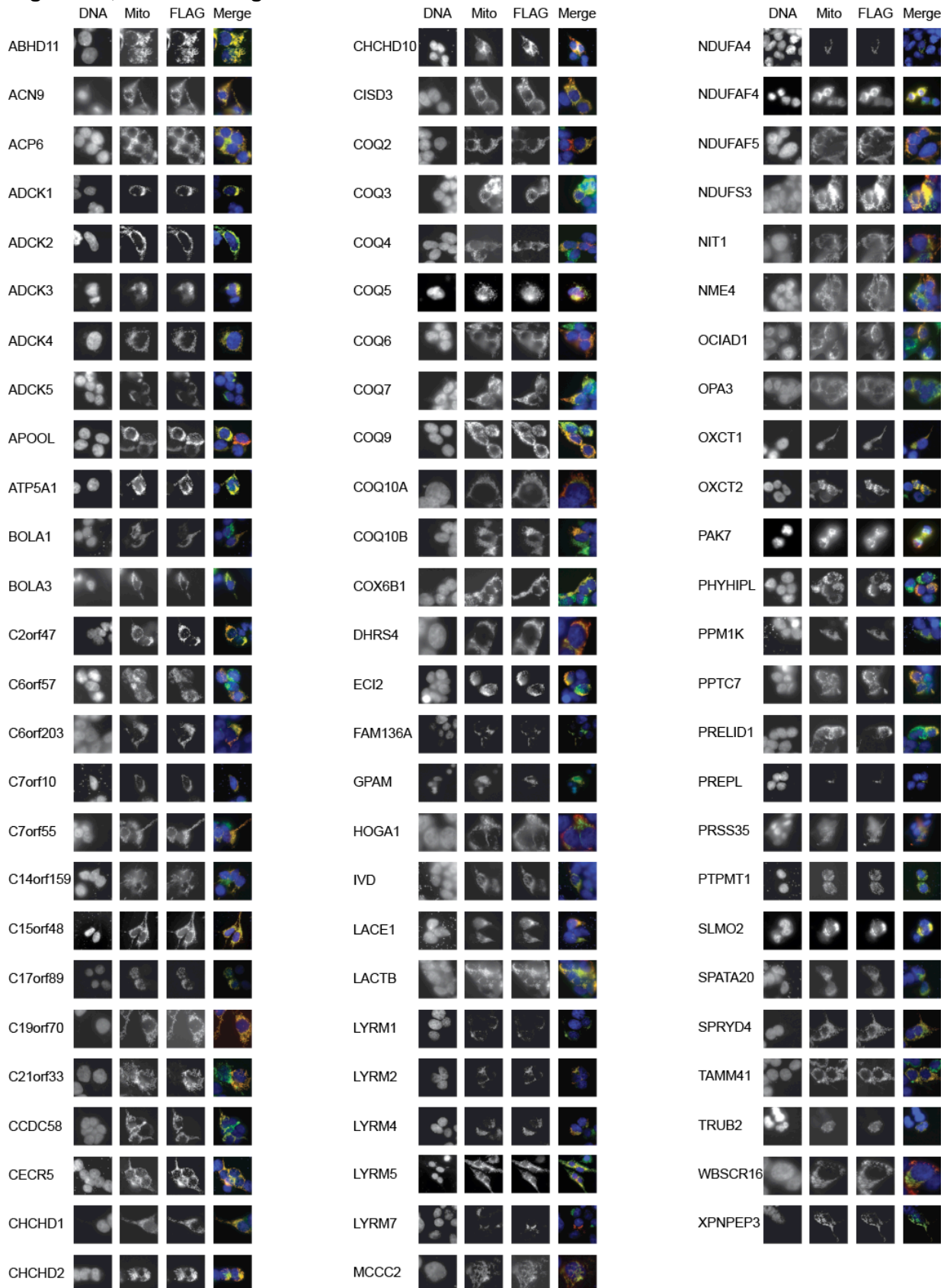


Figure S1, related to Figure 1. Mitochondrial localization of baits used in this study.

Epifluorescence microscopy images showing the mitochondrial localization of all FLAG-tagged baits used in this study. Merged images show the mitochondria-localized GFP signal in green (Mito), the FLAG-tagged protein in red (FLAG) and the nucleus in blue (DNA). Regions of co-localization appear yellow.

Figure S2, related to Figure 2

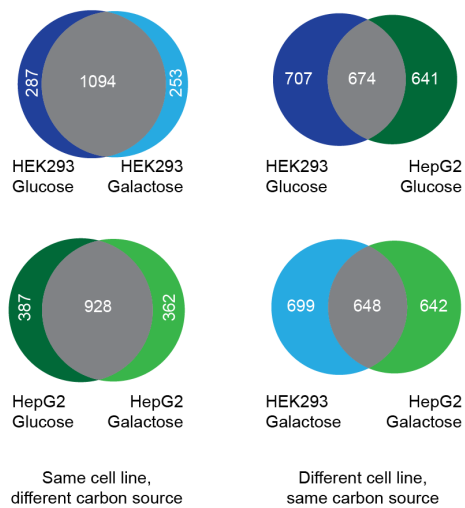


Figure S2, related to Figure 2. Effects of conditions and replicates on AE-MS analyses.

Venn diagrams showing the interactions identified when only subsets of our data are used. Dark blue represents interactions identified in HEK293 cells grown in glucose, light blue is HEK293 in galactose, dark green is HepG2 in glucose, and light green is HepG2 in galactose. Grey represents the overlap in interactions between two groups.

Figure S3, related to Figure 3

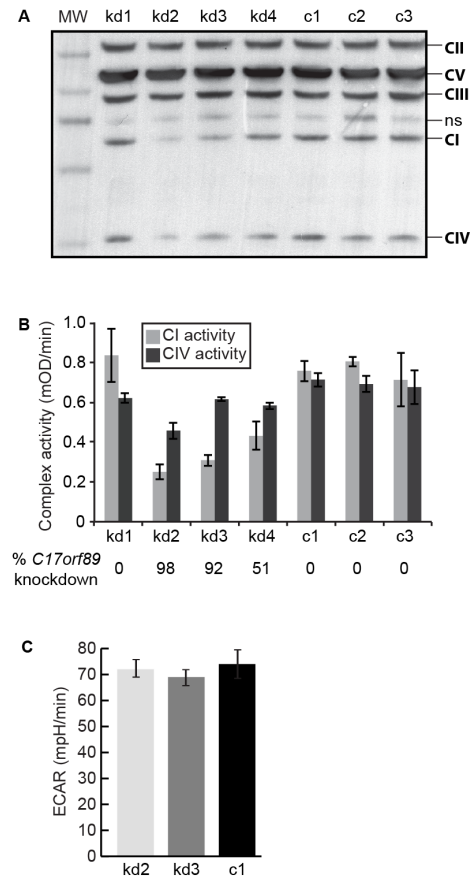


Figure S3, related to Figure 3. Functional assays implicating *C17orf89* in CI assembly.

(A) Abundance of core OxPhos complex subunits in *C17orf89* knock down (kd) and control (c) HEK293 cell lines (ns, non-specific band). Each gel lane is aligned to the activity data in (B).

(B) Complex I (CI) and complex IV (CIV) assays for *C17orf89* knockdown (kd) and control (c) cells as described in Figure 6A of the main text. Error bars indicate \pm standard deviation.

(C) Extracellular acidification rate (ECAR) measurements of *C17orf89* knockdown (kd) and control (c) cells as described in Figure 3D of the main text. Error bars indicate \pm standard error of the mean.

Figure S4, related to Figure 4

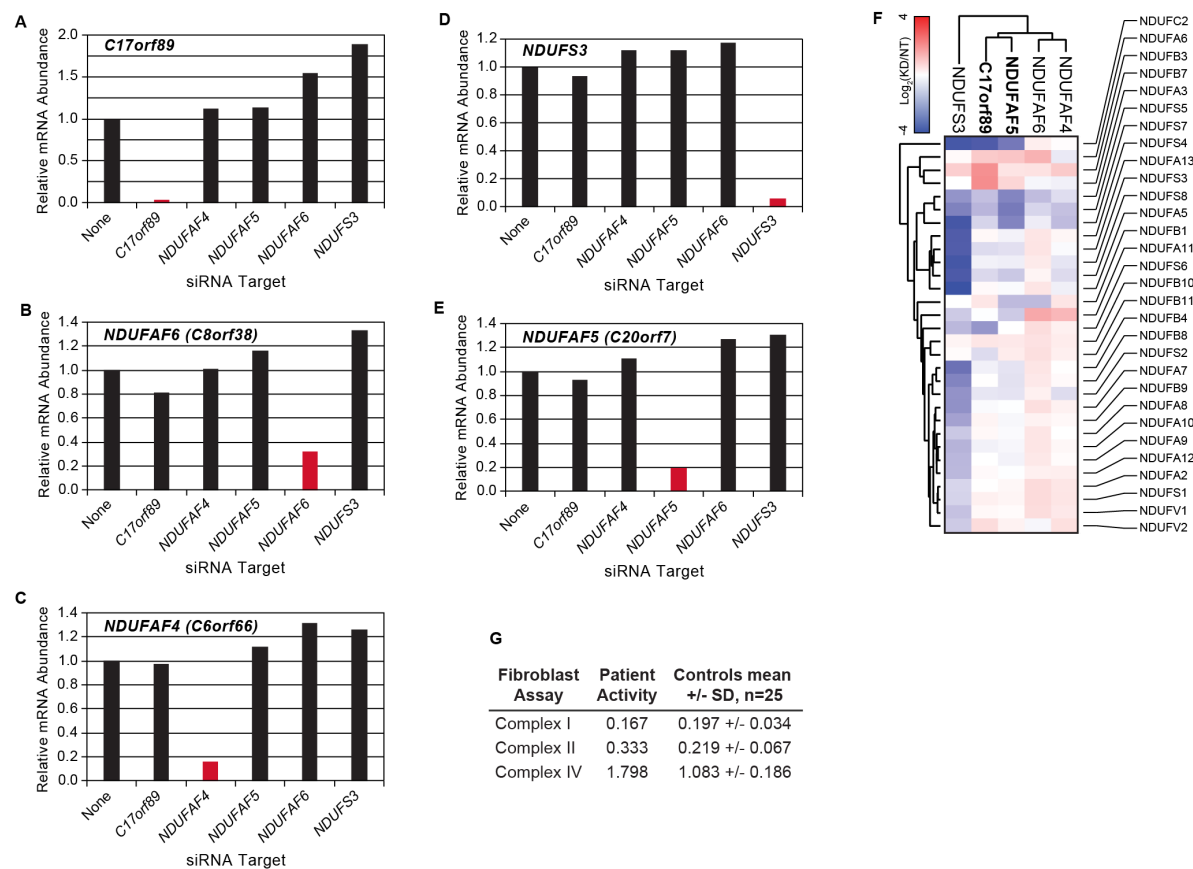


Figure S4, related to Figure 4. Knockdown of *C17orf89* causes a tissue-specific CI defect that is similar to the loss of *NDUF4F5*.

(A-E) Relative mRNA abundance of the indicated siRNA targets across siRNA transfections as assessed by real-time qPCR. (F) Clustered heat map of CI protein subunit levels in CI or CIAF KD cells detected via MS. (G) Respiratory chain complex activity for fibroblasts from patient described in Figure 4.

Figure S5, related to Figure 5

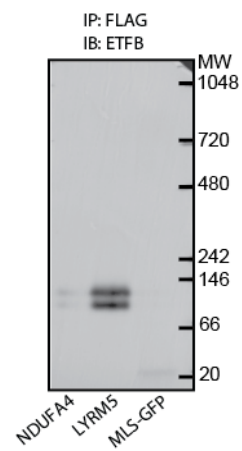


Figure S5, related to Figure 5. ETFB is also present in a complex immunoprecipitated by LYRM5/ETFBP.

The same sample IP eluate shown in Figure 5C was loaded onto a separate native gel and immunoblotted for ETFB.

Figure S6, related to Figure 7

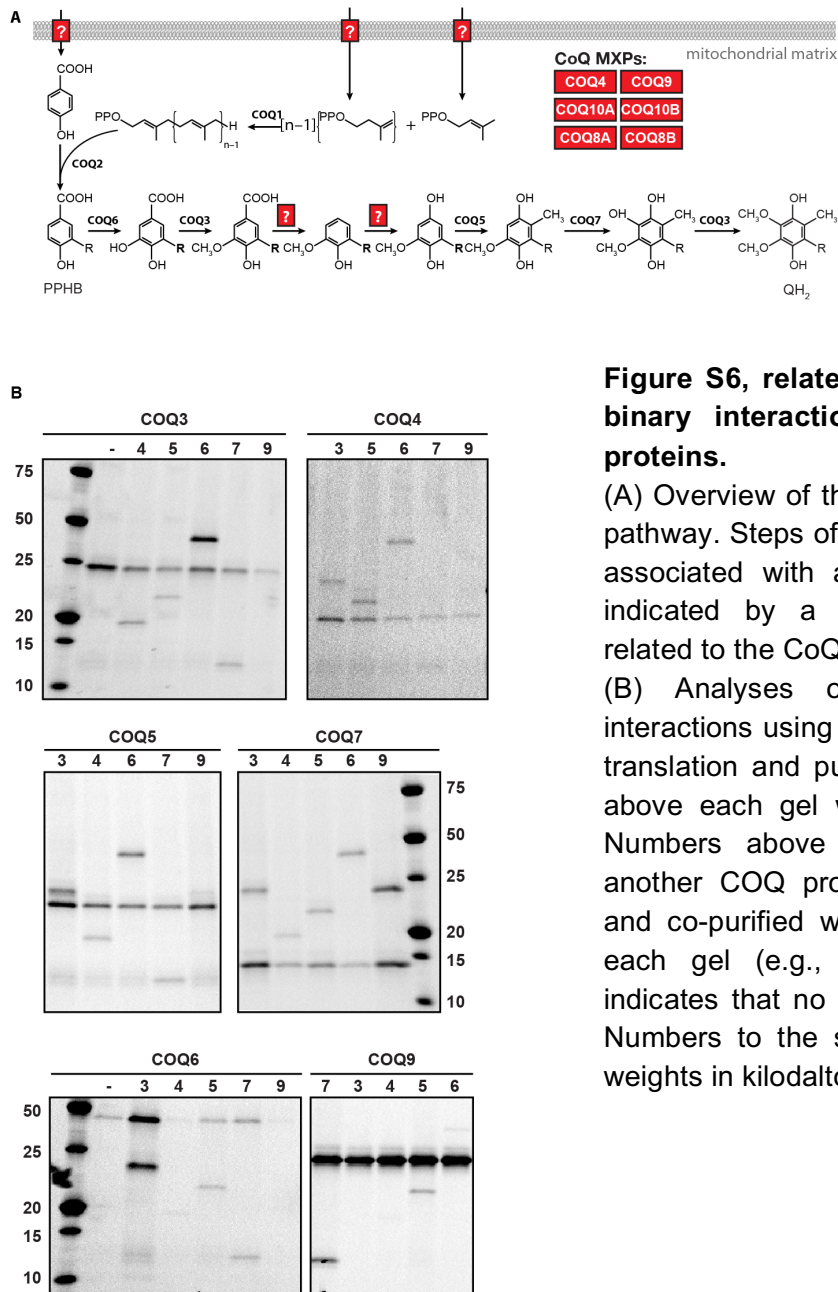


Figure S6, related to Figure 7. Analysis of binary interactions between CoQ-related proteins.

(A) Overview of the coenzyme Q biosynthesis pathway. Steps of the pathway that are not yet associated with a mitochondrial protein are indicated by a question mark (?). MXPs related to the CoQ pathway are boxed in red.

(B) Analyses of COQ protein pairwise interactions using wheat germ cell-free protein translation and purification. The protein listed above each gel was included in each lane. Numbers above each lane correspond to another COQ protein that was co-translated and co-purified with the protein listed above each gel (e.g., "4" indicates "COQ4"; "-" indicates that no other protein was included). Numbers to the sides of gels are molecular weights in kilodaltons.

Figure S7, related to figures 3, 5, and 7

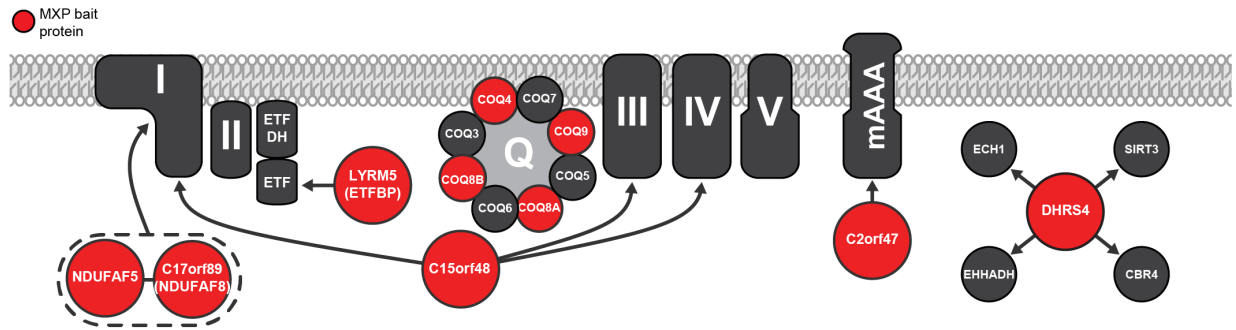


Figure S7, related to figures 3, 5, and 7. Overview of select interactions identified within our data. Red circles indicate MXPs used as bait proteins in this study. Arrows indicate interactions of MXPs with the corresponding mitochondrial proteins or complexes. Complex Q (Q), which involves many interactions identified in this study, is depicted in a simplified form.

SUPPLEMENTAL TABLE LEGENDS

Table S1. MitoCarta+ list, related to Figure 1A and 1B.

Table of our MitoCarta+ list of 1,166 human proteins with validated mitochondrial localization including the 50 MXP's and 27 mitochondrial proteins of known function used as baits in this study.

Table S2. Control PPI list, related to Figure 2A.

Table of literature-established protein-protein interactions (PPIs) involving our positive-control baits.

Table S3. PPIs established in this study, related to Figure 2.

Table of 109,817 PPIs identified in this study, including 1,829 above our CompPASS threshold score.

SUPPLEMENTAL EXPERIMENTAL PROCEDURES

Mitochondrial proteome compilation and disease association

The mouse MitoCarta 2.0 (Mouse.MitoCarta2.0.xls) was downloaded from The Broad Institute (<http://www.broadinstitute.org/pubs/MitoCarta/>) and Entrez GeneIDs were converted from mouse to human using HomoloGene (build 68) and reciprocal BLASTp searches. Data from the mitochondrial matrix (Rhee et al., 2013) and inter-membrane space (Hung et al., 2014) proteomic studies were then integrated with the human MitoCarta. This list of 1,167 human mitochondrial proteins was used as the basis for subsequent determination of subcellular localization. We further annotated these MXPs by assessing their prior association with disease. Many mitochondrial proteins are associated with disease, often with no clear pathological mechanism (Koopman et al., 2012). To connect mitochondrial proteins with their associated pathology, we mapped large-scale disease lists onto our list of mitochondrial proteins (Amberger et al., 2015; Rath et al., 2012; Safran et al., 2010). We found that 368 mitochondrial proteins are associated with more than 300 human disease states. Notably, despite little to no mechanistic knowledge of their function, we observe that mutations in 29 of our MXPs are causal for disease phenotypes as listed in OMIM and many more have been associated with diseases.

Identification of mitochondrial disease-related genes

Disease-gene annotations were downloaded from OMIM (Amberger et al., 2015), Orphanet (Rath et al., 2012) (downloaded March 2015) and GeneCards/MalaCards (Rappaport et al., 2014; Safran et al., 2010) (Koopman et al., 2012).

Generation of tagged constructs

Mitochondrial open reading frames were obtained from The Broad Institute and DNASU (Seiler et al., 2014). Sequences were compared against UniProt (UniProt, 2015) and dbSNP (Sherry et al., 2001). Any remaining mutations of question were assessed for evolutionary conservation using Homologene. Site-directed mutagenesis was performed by QuikChange PCR and primers were designed by PrimerX software: <http://www.bioinformatics.org/primerx/>.

Mammalian cell culture

HEK293 and HepG2 cells were grown in Dulbecco's modified Eagle's medium (DMEM, LifeTechnologies) supplemented with 10% fetal bovine serum and 1% penicillin-streptomycin (LifeTechnologies). Cells were subcultured by trypsinization. On day one, 7 million HEK HepG2 cells were plated in a 15 cm dish and allowed to grow overnight. On day two, cells were transiently transfected with a mix of 20 µg pcDNA3.1 gene-FLAG plasmid, 72 µg linear polyethylenimine (PEI, PolySciences), and 900 µL Opti-MEM (LifeTechnologies). On day four, cells were washed with PBS and media was replaced with DMEM containing 10% FBS, 1% penicillin-streptomycin, and either 10 mM glucose or 10 mM galactose. After 24 hours (Day 5), cells were washed with and harvested into phosphate-buffered saline (PBS), were collected at 2,000 rcf, were snap frozen in liquid nitrogen, and were stored at -80°C.

Subcellular localization analysis

On the day prior to transfection, HEK293 cells were plated at a density of 75,000 cells/well onto poly-D-lysine-coated coverslips in 6-well dishes. Cells were transiently transfected with a mix of 1 µg pcDNA3.1 gene-FLAG, 0.5 µg plasmid encoding green fluorescent protein with an N-terminal mitochondrial localization sequence (MLS-GFP) (Hanson et al., 2004), 7.5 µg PEI, or Lipofectamine LTX Plus (Life Technologies), and 200 µL Opti-MEM. After 24 hours, the cells were fixed (4% paraformaldehyde in PBS), permeabilized (0.2% Triton X-100 in PBS), blocked (1% BSA in PBS), and probed with mouse anti-FLAG M2 1° antibody (F1804, Sigma, 1:2000 (v/v) in 1% BSA in PBS) and either Alexa Fluor 594 or 564-conjugated goat anti-mouse 2° antibody (LifeTechnologies, 1:2000 (v/v) in 1% BSA in PBS) in 1% BSA in PBS. Cells were either counter stained with Hoechst dye (1 µg/mL) to label nuclear

DNA and placed in mounting medium (1:1, v/v, glycerol/PBS), or mounted in ProLong Diamond Antifade Mountant with DAPI (Life Technologies). Epifluorescent microscopy was performed on an Olympus IX81 microscope using 100X oil immersion optics.

Affinity enrichment

Digitonin-based approach

Cell pellets were lysed in 200 μ L cold lysis buffer (20 mM HEPES, pH 7.40, 100 mM NaCl, 10% glycerol, 3% digitonin (Sigma), 1 mM DTT, protease inhibitors (10 μ M benzamide HCl, 1 μ g/mL 1,10-phenanthroline and 0.5 μ g/mL each of pepstatin A, chymostatin, antipain, leupeptin, aprotinin; Sigma), phosphatase inhibitors (500 μ M imidazole, 250 μ M NaF, 300 μ M sodium molybdate, 250 μ M sodium orthovanadate, 1 mM sodium tartrate; Sigma), and deacetylase inhibitors (10 mM each sodium butyrate and nicotinamide; Sigma)), modified from Marbois et al (Marbois et al., 2005). After periodic vortexing on ice, insoluble materials were pelleted (16,000 g, 10 min, 4°C) and the supernatant was retained. The protein concentration was quantified by Bradford assay, and equal masses of cell supernatant were mixed with 30 μ L pre-washed anti-FLAG magnetic beads (Sigma M8823) for 2-3 h at 4°C with end-over-end agitation. Following incubation, beads were washed four times in wash buffer (20 mM HEPES, pH 7.40, 100 mM NaCl, 0.05% digitonin, 10% glycerol) and once in final wash buffer (20 mM HEPES, pH 7.40, 100 mM NaCl). Proteins were eluted in 70 μ L elution buffer (final wash plus 0.2 mg/mL FLAG-peptide) for 30 min at room temperature with constant agitation.

Quantitative mass spectrometry

Protein digestion

Protein pull-downs (40 μ L volume) were transferred from 96-well plates to separate 1.5 mL tubes (Eppendorf) containing 40 μ L of 3 M Urea, 100 mM Tris (pH 8). Protein was reduced with 5 mM dithiothreitol (incubation at 37°C for 45 minutes) and alkylated with 15 mM iodoacetamide (incubation in the dark, at ambient temperature, for 45 minutes). Alkylation was quenched by adding an additional 5 mM dithiothreitol (incubation at ambient temperature for 15 minutes). Protein was enzymatically digested with 0.8 μ g of sequencing-grade trypsin (Promega, Madison, WI) and incubated at ambient temperature overnight. An additional 0.4 μ g of trypsin was added to each sample the next morning and the resulting mixtures were incubated at room temperature for an hour. Digests were quenched by bringing the pH 2 with trifluoroacetic acid and immediately desalted using C18 solid-phase extraction columns (SepPak, Waters, Milford, MA). Prior to washing peptides with 3 mL of 0.1% TFA on the C18 columns, peptides were washed with 1 mL of 5% acetonitrile/0.1% TFA solution to reduce the abundance of the 1x FLAG peptide from each mixture.

CIAF KD cell pellets prepared by pellets were resuspended in 1 mL of 8 M Urea, 40 mM Tris, pH 8, 30 mM sodium chloride, 1 mM calcium chloride and 1 tab protease inhibitor (Roche, Indianapolis, IN). Protein was extracted with 9 mL of methanol (1:10 ratio) and pelleted at 3,500 RPM for 40 minutes. Pellets were air dried for 40 minutes then resuspended in 8 M Urea, 100 mM Tris. Protein concentration was determined through a BCA assay (Thermo Fisher Scientific). Protein (0.5 mg) was reduced with 10 mM TCEP and alkylated with 40 mM chloroacetamide at room temperature. Samples were diluted to 1.5 M Urea with 100 mM Tris, pH 8, and then protein was enzymatically digested with sequencing-grade trypsin in a 1:50 enzyme to protein ratio (Promega, Madison, WI). An additional 1:100 enzyme to protein ratio of sequencing-grade trypsin was added in the morning. Digests were quenched by bringing the pH to 2 with trifluoroacetic acid and immediately desalted using polymeric reversed phase solid-phase extraction columns (StrataX, Phenomenex, Torrance, CA). Peptides were washing with 3 mL of 0.1% TFA and eluted from the columns. Prior to LC-MS/MS analysis, peptide concentration was determined using a quantitative colorimetric peptide assay (Thermo Fisher Scientific).

LC-MS/MS analysis of Protein-Protein interactions

All AE-MS/MS experiments were performed using a NanoAcquity UPLC system (Waters, Milford, MA) coupled to an Orbitrap Elite mass spectrometer (Thermo Fisher Scientific, San Jose, CA). Reverse-phase columns were made

in-house by packing a fused silica capillary (75 μm i.d., 360 μm o.d., with a laser-pulled electrospray tip) with 3.5 μm diameter, 130 \AA pore size Bridged Ethylene Hybrid C18 particles (Waters) to a final length of 30 cm. The column was heated to 55°C for all experiments. Samples were loaded onto the column for 12 minutes in 95:5 buffer A [water, 0.2% formic acid, and 5% DMSO] : buffer B [acetonitrile, 0.2% formic acid, and 5% DMSO] at a flow-rate of 0.40 $\mu\text{L}/\text{min}$. Peptides were eluted using the following gradient: an increase to 22% B over 32 min, followed by a 5 min linear gradient from 22% to 28% B, followed by a 3 min linear gradient from 28% to 70% B which was held for 3 minutes. The column was equilibrated with 5% buffer B for an additional 15 min. Precursor peptide cations were generated from the eluent through the utilization of a nanoESI source. Between each set of baits a 3 run wash sequence was utilized to minimize carryover. The first wash consisted of trapping acetonitrile for 25 minutes and the second was cycle consisted of a 45 min high organic gradient. A pre-blank wash was run by injecting 4.5 μL 0.2% formic acid using the 60 minute gradient described above to allow the identification of carryover proteins.

Mass spectrometry instrument methods consisted of MS¹ survey scans (1×10^6 target value; 60,000 resolution; 300 Th – 1500 Th) that were used to guide fifteen subsequent data-dependent MS/MS scans (2 Th isolation window, HCD fragmentation, normalized collision energy of 30; 5×10^4 target value, 15,000 resolution). Dynamic exclusion duration was set to 45 s, with a maximum exclusion list of 500 and an exclusion width of ± 10 ppm around the selected average mass. Maximum injection times were set to 50 ms for all MS¹ scans and 200 ms for MS/MS scans.

All CIAF KD experiments were performed on a Dionex UPLC system (Thermo Scientific, San Jose, CA) coupled to an Orbitrap Elite mass spectrometer (Thermo Fisher Scientific, San Jose, CA). Reverse-phase columns were made in-house by packing a fused silica capillary (75 μm i.d., 360 μm o.d., with a laser-pulled electrospray tip) with 1.7 μm diameter, 130 \AA pore size Bridged Ethylene Hybrid C18 particles (Waters) to a final length of 30 cm. The column was heated to 65°C.

Samples were loaded onto the column for 6 minutes in 100:0 buffer A [water, 0.2% formic acid, and 5% DMSO] : buffer B [acetonitrile, 0.2% formic acid, and 5% DMSO] at a flow-rate of 0.250 $\mu\text{L}/\text{min}$. Peptides were eluted using the following gradient: an increase to 30% B over 180 min, followed by a 3 min linear gradient from 30% to 100% B, which was held for 3 minutes. The column was equilibrated with 100% buffer A for an additional 20 min. Precursor peptide cations were generated from the eluent through the utilization of a nanoESI source.

Mass spectrometry instrument methods consisted of MS¹ survey scans that were used to guide twenty subsequent data-dependent MS/MS scans. Mass spectrometry instrument methods consisted of MS¹ survey scans (1×10^6 target value; 60,000 resolution; 300 Th – 1500 Th) that were used to guide ten subsequent data-dependent MS/MS scans (2 Th isolation window, CAD fragmentation, normalized collision energy of 35; 5×10^4 target value, ion trap). Dynamic exclusion duration was set to 45 s, with a maximum exclusion list of 500 and an exclusion width of ± 10 ppm around the selected average mass. Maximum injection times were set to 50 ms for all MS¹ scans and 75 ms for MS/MS scans.

All raw files have been deposited to the CHORUS Project (<http://chorusproject.org>), an online repository for sharing, disseminating, and analyzing mass spectrometry data. The AE-MS experiment contains all 936 raw mass spectrometry files from the 6 conditions for each bait, expressed in two different cell lines. The LFQ data contains all 30 files collected from the C17orf89 siRNA lines analyzed. All translated raw files can be viewed directly in a user's web browser or downloaded for sharing, disseminating, and analyzing mass spectrometry data.

Free accounts on Chorus enable users to browse all of the files and download select files or experiments of interest. Otherwise, the full data sets for both categories of experiments can be directly downloaded using the following links:

AE-MS: <https://chorusproject.org/anonymous/download/experiment/b4dd75747a60445d9b3d0d16634e794b>

LFQ: <https://chorusproject.org/anonymous/download/experiment/3dd8e65325734a86b180636f5db2a947>

Data Analysis

Data was also processed using the MaxQuant software suite (Cox and Mann, 2008; Cox et al., 2011). Searches were performed against a target-decoy database (UniProt (human) database, www.uniprot.org, April 4th, 2014, containing the 1X FLAG and MFP-GFP-FLAG sequences) using the default settings for high-resolution mass spectra except for FTMS MS/MS tolerance which was set to 0.015 Da. A maximum of 2 missed tryptic cleavages were allowed. The fixed modification specified was carbamidomethylation of cysteine residues. The variable modification specified was oxidation of methionine. Results were filtered to 1% FDR at the unique peptide level and grouped into proteins within MaxQuant. Proteins were quantified across all replicates within each bait set using MaxLFQ (Cox et al., 2014). Matching between runs was allowed with a retention time window of 1 min.

CompPASS (WD) scoring for protein-protein interactions

We scored our interactions based on CompPASS scores as previously described with a two key changes (Behrends et al., 2010): PPI intensity was measured by averaging the Label free quantification (LFQ) intensity and proteins were grouped to avoid punishing interactions observed multiple times within a single complex.

Briefly the LFQ values from the MaxQuant outputs from all groups of 12 replicates (single bait across cell types and carbon source) were combined. WD scores for the interactions were calculated based on the following equations:

$$WD_{i,j} = \sqrt{(\lambda\omega_j)^p(X_{i,j})} \quad \text{Eq. 1}$$

$$\lambda = \frac{k}{\sum_{i=1}^k f_{i,j}}, \quad f_{i,j} = \begin{cases} 1; & X_{i,j} > 0 \\ X_{i,j} & \end{cases} \quad \text{Eq. 2}$$

$$\omega_j = \frac{\sigma_j}{\overline{X_j}}, \quad \overline{X_j} = \frac{\sum_{i=1}^k X_{i,j}}{k} \quad \text{Eq. 3}$$

$$X_{j,i} = \begin{cases} \text{average intensity of the interaction} \\ \text{between bait } i \text{ and interactor } j \end{cases}$$

$$p = \begin{cases} \text{number of replicates} \\ \text{runs in which} \\ \text{the interactor is present} \end{cases}$$

Where j corresponds to a prey and i corresponds to a bait. k is the total number of different experimental conditions present in the analysis (when all data are used, this number is 78 baits X 2 cell lines X 2 carbon sources = 312.) $f_{i,j}$ indicates if an interaction between a bait (i) and prey (j) is observed ($f_{i,j}=1$) or not ($f_{i,j}=0$.) λ is the reciprocal of frequency indicating the specificity of an interaction, and ω_j is the coefficient of variation for the strength of an interaction (j) across all baits.

A key variation we added to this analysis is the omission of related proteins from the background dataset to improve scoring accuracy for highly interconnected networks. If it is expected that bait A and bait B may be part of the same complex, when λ and ω_j are calculated for bait A, data from bait B is omitted as not to punish interactions from bait A for being present in B (k automatically adjusts for this omission as well). Below is a table of the baits we grouped in this way.

Group Name	Baits
COQ (Lohman et al., 2014)	ADCK3
	ADCK4
	COQ10A
	COQ10B
	COQ2

	COQ3
	COQ4
	COQ5
	COQ6
	COQ7
	COQ9
Complex I (Guarani et al., 2014)	NDUFAF4
	NDUFAF5
	NDUFS3
Ketone Body(Shafqat et al., 2013)	OXCT1
	OXCT2

Protein gels

SDS-PAGE

After competitive elution with FLAG peptide, the eluate was mixed with protein loading buffer and run on a 10% gel for 90 min at 150 V.

Blue Native-PAGE

NativePAGE Novex 4-16% Bis-Tris protein 10-well gels (LifeTechnologies) were prepared with anode buffer (50 mM Bis-Tris) and dark cathode buffer (15 mM Bis-Tris/50 mM tricine, 0.02% Serva Blue G-250). Samples were mixed with NativePAGE sample buffer (LifeTechnologies, BN2003) to 1x final concentration, and were loaded onto gels alongside NativeMARK standard (LifeTechnologies). Gels were run at 150 V for 60 min at 4°C. The dark cathode buffer was then replaced with light cathode buffer (0.002% Serva Blue G-250), and the gels were run for another 60 min at 250 V.

For immunoblotting, gels were transferred to PVDF membranes as below (100 V, 1 h, 4°C). The membrane was then incubated in 8% glacial acetic acid in water for 15 min to fix the proteins. After rinsing with water, methanol was added to the membrane to remove the majority of the Serva Blue stain. Immunoblot proceeded as below.

Immunoblotting

Protein lysates were prepared in RIPA buffer composed of 150 mM NaCl, 1% IGEPAL CA-630, 0.5% sodium deoxycholate, 0.1% SDS, 50 mM Tris (pH 8.0), 0.4 mM EDTA (pH 8.0), 10% glycerol and a protease inhibitor cocktail (Roche Diagnostics), and 20 µg of cleared whole-cell lysate, as determined by BCA assay (Thermo Scientific), was separated on a 4-12% Novex NuPAGE Bis-Tris Mini Gel (Invitrogen), transferred to PVDF and probed with primary antibodies (listed below).

Primary Antibodies used for Immunoblotting

Antigen	Supplier	Product Number
β-actin	Abcam	ab8224
C20orf7 (NDUFAF5)	Abcam	ab192235
CI subunit 8 kDa	Abcam	ab110245
ETF A	Abcam	ab110316
ETF B	Abcam	ab73986
FLAG	Sigma	F1804

NDUFS3	Abcam	ab14711
OxPhos Antibody Cocktail (ATP5A1, SDHA, UQCRC2, NDUFA9, COXIV)	Abcam	ab110412
VDAC	Abcam	ab18988

Generation of *C17orf89* knockdown cells (For Figure 3)

Viral particles of the human lentiviral shRNA *C17orf89* set (TL320977, OriGene, pGFP-C-shLenti backbone) and nonsilencing lentiviral shRNA controls (TR30021, OriGene; shGFP and empty vector in pLKO.1 backbone, The Broad Institute) were produced in HEK293 cells. The hairpin sequences for the *C17orf89* set are: S1: GTTAGAATAAGATGTAAACGGAAGCCACGA, S2: GAAGATGTGACATTCCTCGGTGTTAGATC, S3: TCCAGCATTGTGTCCGTAA-ACCTGAGTTA, S4: GGACTCTGAGCTTCACACCTGTCTGCTGC. Cell transfection was carried out with 5.4 μ L 10 mM polyethylenimine (PEI) per μ g DNA. HEK293T cells (2×10^6) were transfected with 2.5 μ g lentiviral shRNA construct together with 1.625 μ g psPAX2 and 0.875 μ g pMD2.G packaging plasmids. Seventy-two hours after transfection, culture medium containing viral particles was passed through a 0.45 μ m filter, was supplemented with 8 μ g/ml polybrene, and was added to HEK293 target cells for infection. HEK293 cells were transduced in 6-well plates at 1.5×10^5 cells per well. Transduced HEK293 cells were selected in culture medium supplemented with 2 μ g/ml puromycin for at least two weeks. Successful knockdown of *C17orf89* was confirmed by quantitative real-time PCR.

Measurement of Complex I activity.

Abcam's Complex I Enzyme Activity Microplate Assay Kit (ab109721) was used to quantify CI activity in *C17orf89* knock down cell lines. Normalized protein lysate was loaded onto a CI immunocapture plate and incubated for 3 hours at room temperature. The plate was washed and then NADH + reaction dye mixture was loaded on. The plate was read continuously to measure the rate of NADH turnover.

Measurement of oxygen consumption

All respiration assays were performed using an XF-96 Extracellular Flux Analyzer (Seahorse Bioscience) with a 4-port injection system. For initial comparisons of HEK-293 and HepG2 cells, Seahorse 96-well plates were coated with poly-D-lysine, and trypsinized HEK-293 or HepG2 cells were plated at 25,000 cells per well on the day prior to the assay. After calibration of the assay plate using the XF96 software, cells were loaded into the instrument and subjected to a standard mitochondrial stress test protocol. Data analysis was performed using the XF96 software (version 1.4.1.4), and the "Level(Direct)Akos" algorithm that is a built-in factor of the software package.

To test oxygen consumption rate (OCR) and extracellular acidification rate (ECAR) in *C17orf89* knockdown cells, two *C17orf89* knockdown cell lines (S2 and S3) and one control line transfected with a non-silencing vector (S5) were plated on poly-D-lysine coated Seahorse 96-well plates at 25,000 cells per well. After a 24-hr incubation, the growth media were exchanged for XF Assay Medium (Seahorse Biosciences) supplemented with 25 mM glucose (Sigma-Aldrich). OCR and ECAR measurements were taken over 3 minute periods following 1 minute mixing periods. After five initial reads, the cells were treated sequentially with FCCP (Cayman Chemical) to a final concentration of 0.1 μ M, then rotenone (Sigma-Aldrich) to a final concentration of 1.0 μ M, or with equivalent volumes of DMSO as a negative control. Three measurements were taken after each addition.

RNAi For CI assembly factor knock down experiments (for Figure 4)

1 day after seeding, HEK 293 cells were transfected with 10 nM of Dharmacon siGENOME SMARTpools for each target or the Non-Targeting siRNA Control Pool #2 using 0.2% of DharmaFECT 1 Transfection Reagent (GE Healthcare) based on the manufacturer's protocol. After 2 days, the cells were passaged, and the next day were transfected again with 10 nM siRNA, and after another 2 days were collected for real-time qPCR, immunoblot, and mass spectrometry-based proteomic analyses.

Relative Quantification Real Time-qPCR

Total RNA was purified from cultured cells using the RNeasy Mini Kit (QIAGEN). First- strand cDNA was synthesized from purified RNA (500 ng) using the SuperScript III Synthesis System for RT-PCR (Invitrogen). Real time-quantitative PCR was performed using SYBR green-based detection (Applied Biosystems) with *RPLP0* as the endogenous control. Primer sequences are listed below.

Primers used for SYBR Green Real-Time qPCR

SYBR green primers were designed using the Roche Universal ProbeLibrary Assay Design Center tool or the Integrated DNA Technologies (IDT) RealTime qPCR Assay tool.

C17orf89:

Left: ggccgcctgagtaaggac Right: gacagggtggaagctcagagtc

NDUFAF4 (C6orf66):

Left: gctcccagacaccctcta Right: cagctttcatctttacgagca

NDUFAF5 (C20orf7):

Left: gccgaccaaatgtgactacc Right: catatacacggtctgcgatcc

NDUFAF6 (C8orf38):

Left: ctggggcactgaccactac Right: agcagcagggagcataaataa

NDUFS3:

Left: tgcacagttcaaattctctggt Right: cgcagagacaacaggtttaga

RPLP0:

Left: tctacaacctgaagtgttgat Right: caatctgcagacagacactgg

Analysis of CIAF KD lines by mass spectrometry

Protein samples in urea buffer were reduced in 10 mM TCEP and alkylated with 40 mM chloroacetamide at room temperature. Protein was enzymatically digested with sequencing-grade trypsin (Promega, Madison, WI). Digested were quenched by acidification with trifluoroacetic acid and immediately desalted using polymeric reversed phase solid-phase extraction columns (StrataX, Phenomenex, Torrance, CA).

All samples were analyzed using a Dionex UPLC system (Thermo Scientific, San Jose, CA) coupled to an Orbitrap Elite mass spectrometer (Thermo Fisher Scientific, San Jose, CA). Reverse-phase columns were made in-house by packing a fused silica capillary with 1.7 μ m diameter, 130 Å pore size Bridged Ethylene Hybrid C18 particles (Waters) to a final length of 30 cm. The column was heated to 65°C. Precursor peptide cations were generated from the eluent through the utilization of a nanoESI source. Mass spectrometry instrument methods consisted of MS1 survey scans that were used to guide 20 subsequent data-dependent MS/MS scans (see Supplemental Experimental Procedures for further details).

Protein digestion

Cell pellets were resuspended in 1 mL of 8 M Urea, 40 mM Tris, pH 8, 30 mM sodium chloride, 1 mM calcium chloride and 1 tab protease inhibitor (Roche, Indianapolis, IN). Protein was extracted with 9 mL of methanol (1:10 ratio) and pelleted at 3,500 RPM for 40 minutes. Pellets were air dried for 40 minutes then resuspended in 8 M Urea, 100 mM Tris. Protein concentration was determined through a BCA assay (Thermo Fisher Scientific). Protein (0.5 mg) was reduced with 10 mM TCEP and alkylated with 40 mM chloroacetamide at room temperature. Samples

were diluted to 1.5 M Urea with 100 mM Tris, pH 8, and then protein was enzymatically digested with sequencing-grade trypsin in a 1:50 enzyme to protein ratio (Promega, Madison, WI). An additional 1:100 enzyme to protein ratio of sequencing-grade trypsin was added in the morning. Digests were quenched by bringing the pH to 2 with trifluoroacetic acid and immediately desalted using polymeric reversed phase solid-phase extraction columns (StrataX, Phenomenex, Torrance, CA). Peptides were washed with 3 mL of 0.1% TFA and eluted from the columns. Prior to LC-MS/MS analysis, peptide concentration was determined using a quantitative colorimetric peptide assay (Thermo Fisher Scientific).

LC-MS/MS Analysis

All samples were analyzed using a Dionex UPLC system (Thermo Scientific, San Jose, CA) coupled to an Orbitrap Elite mass spectrometer (Thermo Fisher Scientific, San Jose, CA). Reverse-phase columns were made in-house by packing a fused silica capillary (75 μ m i.d., 360 μ m o.d., with a laser-pulled electrospray tip) with 1.7 μ m diameter, 130 Å pore size Bridged Ethylene Hybrid C18 particles (Waters) to a final length of 30 cm. The column was heated to 65°C.

Samples were loaded onto the column for 6 minutes in 100:0 buffer A [water, 0.2% formic acid, and 5% DMSO] : buffer B [acetonitrile, 0.2% formic acid, and 5% DMSO] at a flow-rate of 0.250 μ L/min. Peptides were eluted using the following gradient: an increase to 30% B over 180 min, followed by a 3 min linear gradient from 30% to 100% B, which was held for 3 minutes. The column was equilibrated with 100% buffer A for an additional 20 min.

Precursor peptide cations were generated from the eluent through the utilization of a nanoESI source.

Mass spectrometry instrument methods consisted of MS1 survey scans that were used to guide twenty subsequent data-dependent MS/MS scans. Mass spectrometry instrument methods consisted of MS1 survey scans (1x10⁶ target value; 60,000 resolution; 300 Th – 1500 Th) that were used to guide ten subsequent data-dependent MS/MS scans (2 Th isolation window, CAD fragmentation, normalized collision energy of 35; 5x10⁴ target value, ion trap). Dynamic exclusion duration was set to 45 s, with a maximum exclusion list of 500 and an exclusion width of \pm 10 ppm around the selected average mass. Maximum injection times were set to 50 ms for all MS1 scans and 75 ms for MS/MS scans.

Coenzyme Q Quantification

A frozen pellet of tissue culture cells (isolated from a 20 cm plate at 80–100% confluence) was thawed on ice, mixed with glass beads (0.5 mm diameter, 100 μ L) and H₂O (400 μ L, 4 °C), and vortexed (4 x 30 s) to lyse the cells. A portion of the cell lysate (containing 2 mg of protein, as determined by a BCA assay) was mixed with H₂O (to a total volume of 200 μ L), spiked with an internal standard (CoQ₆, 20 μ L, 10 μ M), and mixed by vortexing (30 s). CHCl₃/MeOH (1:1, v/v) (900 μ L) was added and vortexed (3 x 30 s). The samples were centrifuged (3,000 g, 3 min, 4 °C) to complete phase separation. 600 μ L of the lower organic phase was transferred to a clean tube. HCl (1 M, 100 μ L, 4 °C) was added to the remaining aqueous phase and vortexed (30 s). CHCl₃/MeOH (1:1, v/v) (400 μ L) was added and vortexed (2 x 30 s). The samples were centrifuged (3,000 g, 3 min, 4 °C) to complete phase separation. The lower organic phase was combined with the previous organic extract, and the combined extracts were dried under Ar_(g). The organic residue was reconstituted in ACN/IPA/H₂O (65:30:5, v/v/v) (100 μ L) by vortexing (2 x 30 s).

Lipids from 10 μ L of extract were separated by LC on an Ascentis Express C18 column (150 mm x 2.1 mm x 2.7 μ m particle size, Supelco, Bellefonte, PA) using an Accela HPLC pump (Thermo Scientific, San Jose, CA) at a flow-rate of 0.5 mL/min using a linear gradient. Mobile phase A was 70/30 acetonitrile/water containing 10 mM ammonium acetate and 0.025% acetic acid and B was 90/10 isopropanol/acetonitrile containing the same additives. Initially the flow was maintained at 50% B for 1.5 min, then ramped to 95% B over 6.5 min, held there for 2 min before returning to starting conditions over 1 min, and finally re-equilibrating the column for 2.5 min. The auto sampler (HTC PAL, Thermo Scientific) vigorously mixed each sample before injection to ensure homogeneity. Quantitation was performed using tandem mass spectrometry by integrating the peak area of the 880.72 \rightarrow 197.08 Th transition of coenzyme Q₁₀ and normalizing to the 591.44 \rightarrow 197.08 Th transition of the internal standard coenzyme Q₆ using the Xcalibur software suite (Thermo Scientific, Version 3.0). MS conditions were as follows: a Q Exactive

mass spectrometer (Thermo Scientific, Build 2.5) equipped with a HESI II spray source kept at 350 °C and +4 kV was used for detection. The inlet capillary was kept at 350 °C, sheath gas was set to 60 units, and auxiliary gas to 20 units. Resolving power was set to 35,000, AGC target to 2×10^5 , isolation width to 1 Th, normalized collision energy to 27 units, and maximum injection time to 375 ms.

Cell-free expression and purification.

Plasmid DNA was treated with 0.05 µg/µL proteinase K to remove trace amounts of RNase, purified, and used as individual transcription templates with SP6 RNase polymerase. Transcription and translation methods are as previously described (Makino et al., 2013). Briefly, transcription reactions included 0.2 mg/mL DNA, 20 mM magnesium acetate, 2 mM spermidine trihydrochloride, 10 mM DTT, 80 mM Hepes-KOH, pH 7.8, 4 mM each NTP, pH 7.0, 1.6 U/µL SP6 RNA polymerase (Promega), and 1 U/µL RNasin (Promega). Transcriptions were incubated for 4 h at 37°C. Nonpurified transcription reactions were used singly or mixed in equal volumes for multi-protein interaction monitoring and added to wheat germ extract (WEPRO2240; CellFree Sciences) in a standard dialysis cup reaction (Makino et al., 2013). Each 25 µL reaction contained 60 O.D. wheat germ extract (6.25 µL), 24 mM Hepes-KOH, pH 7.8, 100 mM potassium acetate, 6.25 mM magnesium acetate, 0.4 mM spermidine trihydrochloride, 4 mM DTT, 1.2 mM ATP, 0.25 mM GTP, 16 mM creatine phosphate, 0.0005% sodium azide, 0.04 mg/mL creatine kinase, 0.3 mM each amino acid (amino acid mixture adjusted to pH 7.0 with KOH), and 5 µL of RNA. Thirty-two-fold excess dialysis buffer was used for each reaction, containing all reaction components except for wheat germ extract, creatine kinase, and RNA. After assembly of dialysis cups and 18-h incubation at 23°C, duplicate translations (50 µL) of each combination were pooled and centrifuged for 5 min at 20,000 rcf at 10°C. The soluble fraction was removed and added to 20 µL of StrepTactin resin equilibrated in 25 mM Hepes, pH 7.8, 150 mM NaCl, and 1 mM DTT in a 96-well filter plate (HTS Multiscreen; Millipore). The resin with bound protein was washed three times with 150 µL of binding buffer. Strep(II)-tagged protein and protein complexes were eluted in 2.5 mM desthiobiotin in the same buffer. Bound samples were eluted by increasing the imidazole concentration to 500 mM. Samples of the StrepTactin elutions were loaded without heating on 4-20% Stain-free TGX Criterion gels (Bio-Rad) and subjected to denaturing SDS/PAGE. Gels were imaged by tryptophan fluorescence using a Bio-Rad Stain Free Imager, followed by staining in Coomassie Brilliant Blue R-250.

SUPPLEMENTAL REFERENCES

- Amberger, J.S., Bocchini, C.A., Schiettecatte, F., Scott, A.F., and Hamosh, A. (2015). OMIM.org: Online Mendelian Inheritance in Man (OMIM®), an online catalog of human genes and genetic disorders. *Nucleic Acids Research* 43, D789-798.
- Behrends, C., Sowa, M., Gygi, S., and Harper, J. (2010). Network organization of the human autophagy system. *Nature* 466, 68-U84.
- Cox, J., Hein, M.Y., Lubner, C.A., Paron, I., Nagaraj, N., and Mann, M. (2014). Accurate proteome-wide label-free quantification by delayed normalization and maximal peptide ratio extraction, termed MaxLFQ. *Mol Cell Proteomics* 13, 2513-2526.
- Cox, J., and Mann, M. (2008). MaxQuant enables high peptide identification rates, individualized p.p.b.-range mass accuracies and proteome-wide protein quantification. *Nature biotechnology* 26, 1367-1372.
- Cox, J., Neuhauser, N., Michalski, A., Scheltema, R.A., Olsen, J.V., and Mann, M. (2011). Andromeda: a peptide search engine integrated into the MaxQuant environment. *Journal of proteome research* 10, 1794-1805.
- Guarani, V., Paulo, J., Zhai, B., Huttlin, E.L., Gygi, S.P., and Harper, J.W. (2014). TIMMDC1/C3orf1 functions as a membrane-embedded mitochondrial complex I assembly factor through association with the MCIA complex. *Mol Cell Biol* 34, 847-861.
- Hanson, G.T., Aggeler, R., Oglesbee, D., Cannon, M., Capaldi, R.A., Tsien, R.Y., and Remington, S.J. (2004). Investigating mitochondrial redox potential with redox-sensitive green fluorescent protein indicators. *The Journal of biological chemistry* 279, 13044-13053.
- Hung, V., Zou, P., Rhee, H.-W., Udeshi, N.D., Cracan, V., Svinkina, T., Carr, S.A., Mootha, V.K., and Ting, A.Y. (2014). Proteomic Mapping of the Human Mitochondrial Intermembrane Space in Live Cells via Ratiometric APEX Tagging. *Molecular cell*.
- Koopman, W.J.H., Willems, P.H.G.M., and Smeitink, J.A.M. (2012). Monogenic Mitochondrial Disorders. *New England Journal of Medicine* 366, 1132-1141.
- Lohman, D.C., Forouhar, F., Beebe, E.T., Stefely, M.S., Minogue, C.E., Ulbrich, A., Stefely, J.A., Sukumar, S., Luna-Sanchez, M., Jochem, A., *et al.* (2014). Mitochondrial COQ9 is a lipid-binding protein that associates with COQ7 to enable coenzyme Q biosynthesis. *Proc Natl Acad Sci U S A* 111, E4697-4705.
- Makino, S.-i., Beebe, E.T., Markley, J.L., and Fox, B.G. (2013). Cell-Free Protein Synthesis for Functional and Structural Studies. In (Totowa, NJ: Humana Press), pp. 161-178.
- Marbois, B., Gin, P., Faull, K.F., Poon, W.W., Lee, P.T., Strahan, J., Shepherd, J.N., and Clarke, C.F. (2005). Coq3 and Coq4 define a polypeptide complex in yeast mitochondria for the biosynthesis of coenzyme Q. *J Biol Chem* 280, 20231-20238.
- Rappaport, N., Twik, M., Nativ, N., Stelzer, G., Bahir, I., Stein, T.I., Safran, M., and Lancet, D. (2014). MalaCards: A Comprehensive Automatically-Mined Database of Human Diseases. *Current protocols in bioinformatics* 47, 1.24.21-21.24.19.
- Rath, A., Olry, A., Dhombres, F., Brandt, M.M., Urbero, B., and Ayme, S. (2012). Representation of rare diseases in health information systems: the Orphanet approach to serve a wide range of end users. *Human mutation* 33, 803-808.
- Rhee, H.-W., Zou, P., Udeshi, N.D., Martell, J.D., Mootha, V.K., Carr, S.A., and Ting, A.Y. (2013). Proteomic mapping of mitochondria in living cells via spatially restricted enzymatic tagging. *Science (New York, NY)* 339, 1328-1331.
- Safran, M., Dalah, I., Alexander, J., Rosen, N., Iny Stein, T., Shmoish, M., Nativ, N., Bahir, I., Doniger, T., Krug, H., *et al.* (2010). GeneCards Version 3: the human gene integrator. *Database* 2010, baq020-baq020.
- Seiler, C.Y., Park, J.G., Sharma, A., Hunter, P., Surapaneni, P., Sedillo, C., Field, J., Algar, R., Price, A., Steel, J., *et al.* (2014). DNASU plasmid and PSI:Biological-Materials repositories: resources to accelerate biological research. *Nucleic Acids Research* 42, D1253-1260.

Shafqat, N., Kavanagh, K.L., Sass, J.O., Christensen, E., Fukao, T., Lee, W.H., Oppermann, U., and Yue, W.W. (2013). A structural mapping of mutations causing succinyl-CoA:3-ketoacid CoA transferase (SCOT) deficiency. *J Inherit Metab Dis* 36, 983-987.

Sherry, S.T., Ward, M.H., Kholodov, M., Baker, J., Phan, L., Smigielski, E.M., and Sirotkin, K. (2001). dbSNP: the NCBI database of genetic variation. *Nucleic Acids Research* 29, 308-311.

UniProt, C. (2015). UniProt: a hub for protein information. *Nucleic Acids Res* 43, D204-212.